Studies on modifications of glass structure using ultrafast pulse laser

Kiyotaka MIURA

2003

STUDIES ON MODIFICATIONS OF GLASS STRUCTURE USING ULTRAFAST PULSE LASER

KIYOTAKA MIURA

2003

DEPARTMENT OF MATERIAL CHEMISTRY
GRADUATE SCHOOL OF ENGINEERING
KYOTO UNIVERSITY

Contents

General Introduction

The reactions between light and glass materials have been well studied in photochromic, photosensitive, and polychromatic glasses [1-3]. There have also been considerable researches on the writing of Bragg gratings inside optical fibers and on photochemical hole burning [4-6]. The reactions between light and glasses have been put to practical use in phase-change-type memories using a heat-mode scheme [7]. Such reactions are usually produced by exciting an absorption area on the glass to attain various types of light-induced structural changes. Actually, continuous-wave lasers and pulse lasers having pulse widths of nanosecond or longer order are used as light sources, and the laser wavelengths are mostly used in the ultraviolet regions. As a consequence, light-induced reactions are more active on the surface layer of the glass; it is difficult to achieve light-induced effects only in selective internal areas of the glass, since these light are absorbed in glasses.

In general, it is difficult to produce an interaction effect between glasses and light by one photon process when the excitation wavelength does not agree with the wavelength of absorption region of glasses. However, various types of interactions with glasses can be produced by using an ultrashort-pulse laser operating at the nonresonance wavelength with pulse widths of femtosecond order [8,9]. Ordinally, ultrashort laser pulses are used mainly for high-time resolution observation and evaluation of the dynamics of the phenomena that occur within materials on time scales ranging from picoseconds to femtoseconds. Such phenomena include a direct interaction between light and atoms or molecules, a saturation process associated with the

coherent state of materials, and an elementary process of chemical reactions. By using a short pulse width of femtosecond laser an extremely high peak power can be also obtained. so high intensity light (up to 10^{14} W/cm^2) can easily be achieved by focusing the laser beam. From a practical point of view, this high laser intensity offers new challenges and provides new phenomena.

When the absorption mechanisms described above give sufficient energy into the material, permanent damage is produced. For pulse durations longer than a few tens of picoseconds, energy is transfered from the laser-excited electrons to the lattice on the time scale of the pulse duration. This energy is then carried out of the focal volume by thermal diffusion. Damage occurs when the temperature of the material in the irradiated region becomes high enough for the material to melt or fracture [10]. For pulses shorter than a few picoseconds, the mechanism for optical damage is simpler than the longer laser pulses. Absorption occurs on a time scale that is shorter compared to the time scale for energy transfer to the lattice, decoupling the absorption and lattice heating processes [11]. Electrons in the conduction band are heated by the laser pulse much faster than the cooling by electron-phononcoupling emissions. The electron density grows through avalanche ionization until the plasma frequency approaches the frequency of the incident laser radiation [11]. This high density plasma strongly absorbs laser energy by free-carrier absorption. This shock-like deposition of energy, on a time scale much shorter than the thermal diffusion time, leads to the ablation of materials on the surface or permanent structural change in the bulk glasses.

The availability of laser pulses with femtosecond duration allows materials to be subjected to a higher laser intensity than ever before, opening the door to the study of light/glass interactions in a new regime. Therefore, the development of high-energy-density femtosecond-pulse lasers has prompted us to investigate the unexplored potential for

inducing multiphoton photochemical reactions. We have used a femtosecond laser with an ultrahigh-strength electric field as one of our tools to make microscopic modifications in glasses and to realize the novel function of glasses. The fabrication process involves focusing near-infrared femtosecond laser pulses inside a bulk glass to induced microscopic modification at the focal point of the laser beam. When the glass is translated with respect to focal point, complex three-dimensional microscopic modifications can be fabricated inside the bulk glass substrate. There is therefore considerable interest in using femtosecond lasers to generate various types of microscopic which are of scientific and practical interest.

We found that refractive index changes of the order from 10^{-2} to 10^{-3} can be induced within various types of glass by irradiating the glass with focused femtosecond laser pulses [12]. By using a femtosecond laser with a high repetition rate, permanent optical waveguides can be successfully written in various glasses, where refractive index changes are continuously induced along a path traversed by focal point [13,14].

We have also attempted the effect of laser irradiation in rare-earth ions doped glasses by femtosecond laser pulses. It was discovered that the long-lasting phosphorescence phenomenon which can be observed with human eye even for 10 hours after the stop of the exiting [15]. Photo-reductions of rare earth ions in a few glasses could also be produced by the irradiation of femtosecond laser pulses. Up to now, to our knowledge, no creation of permanent photo-reduction in the glass have been reported with the laser, although several investigations have been conducted on the transient creation of the divalent rare earth ions in solutions and halide crystals by laser irradiation [16,17]. In addition, by using the valence state change of samarium ions to make a "bit", it was proved that data can be read out as fluorescence information and erased by the irradiation with a CW laser. This technique will be useful in fabricating next-generation 3D optical memory devices with an

ultrahigh storage density.

Various nonlinear optical effects such as multiphoton ionization and plasma vibration were induced in the focused area of the laser beam, resulting in a dramatic rise in the temperature and internal pressure in the region of focus. In taking advantage of this phenomenon, we could form spherical melting regions at arbitrary sites within a bulk glass by using a femtosecond laser with a high repetition rate, and for the first time to our knowledge, we have succeeded in growing a crystal with single-crystal-like structure inside glasses.

In the present study, several effects and mechanisms of microscopic modifications in glasses induced by 800 nm femtosecond pulse laser are investigated. It is confirmed that a variety of microscopic modifications which are permanent or metastable at room temperature can be made only in the laser focusing area inside transparent glasses by using femtosecond laser pulses.

In Chapter 1, mechanisms and applications of the laser-induced refractive index change of the glass are presented. Here, the structural change in the silica glasses before and after the laser irradiation is also discussed. Electron spin resonance (ESR) measurement and confocal microscopic Raman spectroscopy was used to investigate for the photo-induced refractive index change found in SiO_2 glass and to reveal the mechanism on this phenomenon. The preparation and optical characterization of photo-written optical waveguides formed in various glasses are also described.

In Chapter 2, studies regarding the generation of induced structures using rare-earth ions are presented, including long-lasting phosphorescence and permanent photoreduction in glasses. Here, a three-dimensional long-lasting phosphorescence phenomenon in calcium alumino-silicate glasses doped with Ce^{3+}, Tb^{3+}, and Pr^{3+} induced with a femtosecond laser is presented. The space selective photo-reduction of Sm^{3+} to Sm^{2+} inside sodium aluminoborate glasses is presented. The

possibility of achieving three-dimensional optical data storage with rewritable and ultrahigh density by using permanently photoreduction of samarium ions induced with a femtosecond laser is examined.

In chapter 3, space-selective growth of econd-harmonic-generation BBO (β-BaB_2O_4) crystals inside BaO-Al_2O_3-B_2O_3 glass samples at the focal point of 800-nm femtosecond laser beam is presented. A spherical heated region was formed during the focused laser irradiation through observation with an optical microscope. The generation of a fiber BBO single crystal continuously inside the glass is attempted by moving the spherical melting zone.

References

[1] N. F. Borreli and B. Wedding, J. Appl. Phys. **63,** 15, (1988).

[2] D. C. Boyd and J. F. MacDowell, *Commercial Glasses, Advance in Ceramics* **18**, 165, (1986).

[3] N. F. Borrelli, J. B. Chodak, D. A. Nolan, and T. P. Seward, *J. Opt. Am.* **69**, 1514, (1979).

[4] K. O. Hill, Y. Fujii, D. C. Johnson, and B. S. Kawasaki, *Appl. Phys. Lett.* **32**, 647, (1978).

[5] P. Cordier, J. C. Doukhan, E. Fertein, P. Bernage, P. Niay, J. F. Bayon, and T. Georges, *Opt. Commun.* **111**, 269, (1994).

[6] K.Hirao, *J. Non-Cryst. Solids* **196**, 16, (1996).

[7] M. Terao, T. Nishida, Y. Miyauchi, S. Horigome, T. Kaku, and N. Ohta, *Proc. SPIE* **695**, 105, (1986).

[8] E. N. Glezer, M. Milosavljevic, L. Huang, R. J. Finlay, T.-H. Her, J. P. Callan, and E. Mazur, *Opt. Lett.* **24**, 2023, (1996).

[9] Y. Kondo, T Suzuki, H. Inouye, K. Miura, T. Mitsuyu, and K. Hirao, Jpn. *J. Appl. Phys.* **37**, 94, (1998).

[10] B. C. Stuart, M. D. Feit, S. Herman, A. M. Rubenchik, B. W. Shore, and M. D. Perry, *J. Opt. Soc. Am. B* **13**, 459 (1996).

[11] B. C. Stuart, M. D. Feit, S. Herman, A. M. Rubenchik, B. W. Shore, and M. D. Perry, *Phys. Rev. B* **53**, 1749 (1996).

[12] K. M. Daivis, K. Miura, N. Sugimoto, and K. Hirao, *Opt. Lett.* **21**, 1729, (1996).

[13] K. Miura, J. Qiu, H. Inouye, T. Mitsuyu, and K. Hirao, *Appl. Phys. Lett.* **71**, 3329, (1997).

[14] K. Miura, H. Inouye, J. Qiu, and K. Hirao, *Nuclear Instruments and Methods in Physics Research* B **141**, 726, (1998).

[15] J. Qiu, K. Miura, H. Inouye, Y. Kondo, T. Mitsuyu, and K. Hirao, *Appl. Phys. Lett.* **73**, 1763, (1998).

[16] M. Kusaba, N. Nakashima, Y. Izawa, C. Yamada, and W. kawamura,

Chem. Phys. Lett. **221**, 407, (1994).
[17] Y. Yamada and S. Ohno, *Chemistry Lett.* 465, (1991).

Chapter 1

Mechanisms and applications of laser-induced refractive index change of glasses by femtosecond laser irraduation

1.1 Photo-refractive index changes with femtosecond laser (fs) pulses

1.1.1 Introduction

Since the 1970's, many investigations of the effects of UV radiation damage in high-silica glasses (especially Ge-doped silica glass) have been performed with the objective of producing optical devices (e.g., Bragg gratings) in fibers and thin films [1]. In contrast, laser damage by visible and IR laser light has received little attention owing to the low photon energy at these wavelengths. The development of high-energy-density femtosecond pulse lasers, however, has prompted us to investigate the unexplored potential for inducing multiphoton photochemical reactions and optical devices in glass by use of lasers of sub-UV photon energy.

In this section, it was presented results that visible laser damage and photoinduced refractive-index changes can be achieved with a red visible femtosecond laser.

1.1.2 Experimental procedure

By using the apparatus shown in Fig. 1.1, the irradiation sources employed were a regeneratively amplified 800-nm Ti:sapphire laser that emitted 1kHz or 200-kHz, mode-locked pulses. The average power of the laser beam at the sample location was controlled between approximately

40 and 800 mW by neutral-density filters that were inserted between the laser and the microscope objective. The 5-mm-diameter beam was focused through 5-20× microscope objectives and injected into polished plates of dry and wet silica, Ge-doped silica, borate, soda lime silicate, and fluorozirconate (ZBLAN) glasses. With the help of an XYZ stage, the samples were translated at rates of 100-10,000 μm/s either parallel or perpendicular to the incident laser beam, thus creating visible damage lines inside the glasses.

For the silica and the Ge-doped silica glasses, we made cross sections of the damage lines by cutting the samples and polishing the exposed surfaces. Refractive-index profiles of the cross sections were measured with a optiprove. For UV and electron spin resonance (ESR) spectroscopic measurements, we took scans before and after we wrote identical damage line patterns in glass plates by using a 10× microscope objective and translating the samples perpendicular to the incident light at a rate of 100 μm/s. For these samples, the average laser power at the sample was ~470mW. Assuming a square-wave pulse, a uniform beam intensity, and a diameter of the laser focal point that is equal to the thickness of the observed damage lines (~6 μm), we found that the samples experienced 12,000 pulses/spot, and each spot was subjected to a dose of 100 MJ/cm^2 during a single pass of the laser.

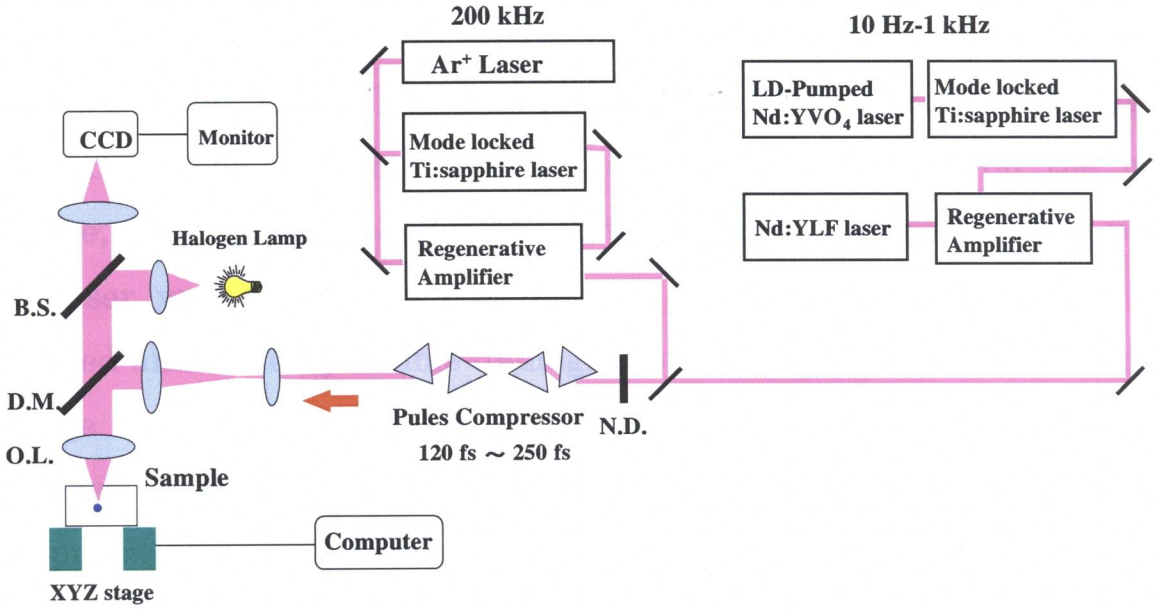

Fig. 1.1. Schematic diagram of photo-induced refractive index changees by a femtosecond laser

1.1.3 Results and Discussion

1.1.3.1 Photo-induced refractive index change with fs laser pulses

The damage caused by focusing 50-μJ, 150-fs 1-kHz mode-locked pulses on the surface of the fluoride glass samples is shown in Fig. 1.2 (a), and the damage caused by focusing pulses in the interior of the samples is shown in Fig. 1.2 (b). Each sample received 2000 pulses/spot through a 10X microscope objective. When the laser was focused on the near surface, ablation or cracking due to thermal shock occurred. But when the laser was focused in the interior of the glass, no cracking was detected and the only visible damage resulting from the refractive-index change was observed at the focal points. In this case, the spot size decreased with the number of irradiations and with the peak power of the pulses. Figure 1.3 shows an array of the refractive index changes inside silica glass induced by a single pulse for each, where peak power was 10^9 W/cm^2. These spots have diameters of roughly 400 nm, as measured with a confocal laser scanning microscope. This was significantly smaller than the focal-beam size and the wavelength of the laser (800 nm). This may be due to the self-focusing of the laser and non-linear effect of the glass, which resulted from the interaction between the laser and the glass.

In general, it is difficult to produce an interaction between glass and a laser when the pulse energy is not absorbed by a one photon absorption process. However, an ultrashort-pulse laser can produce various types of interactions in various types of glass through the non-linear optical process. In practice, white-light generation due to the self-phase modulation and second-harmonic generation were observed from the focal point of the laser beam inside the glass.

Typical emission spectra of fluoride glass and Ge-doped silica glass during irradiation from an ultrashort-pulse laser are shown in Fig. 1.4; the laser wavelength and average power were 800 nm and 200 mW at 200 kHz, respectively. Thus various nonlinear processes occur at a focal point. By using the photosensitivity attributed to the nonlinear optical process, we were able to induce refractive-index changes in only the focus region because nonlinearity occurs only in regions where the optical intensity is above the damage threshold.

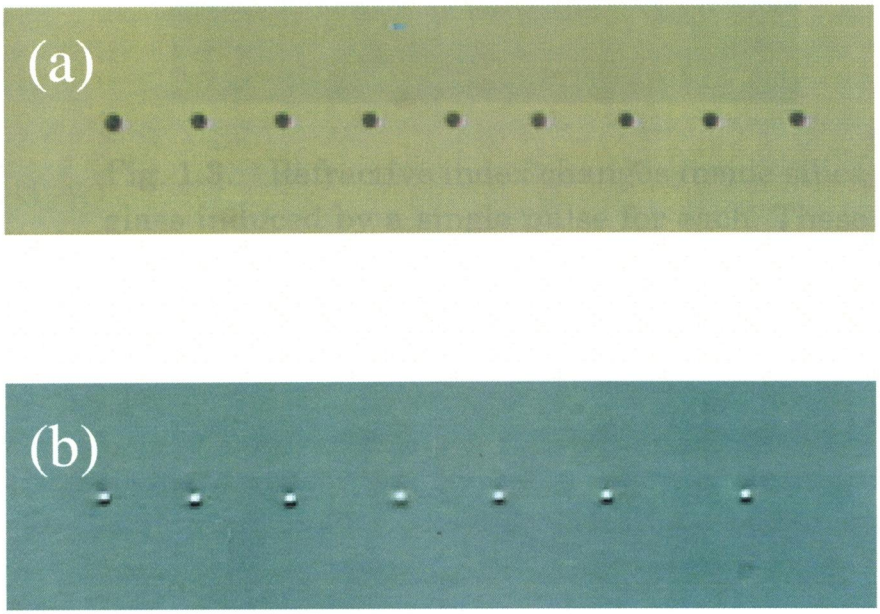

Fig. 1.2. Damages caused by focusing a femtosecond laser (a) on the surface of the fluoride glass samples, and (b) in the interior of the samples.

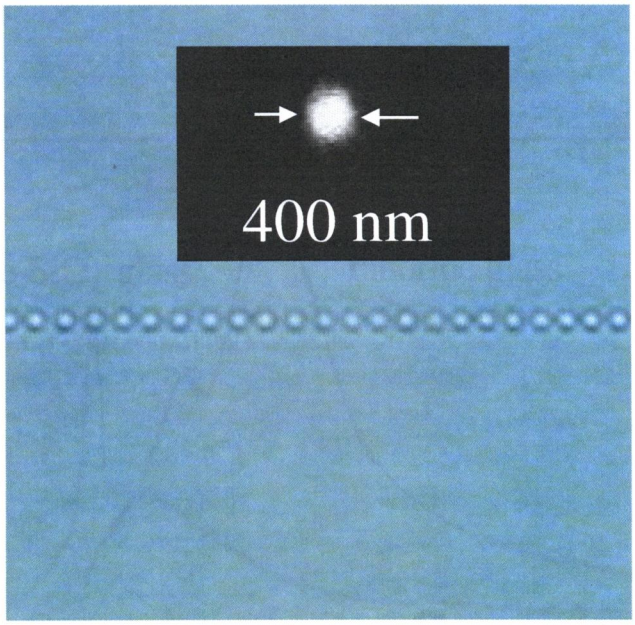

Fig. 1.3. Refractive index changes inside silica glass induced by a single pulse for each. These spots have diameters of roughly 400 nm, as measured with a confocal laser scanning microscope.

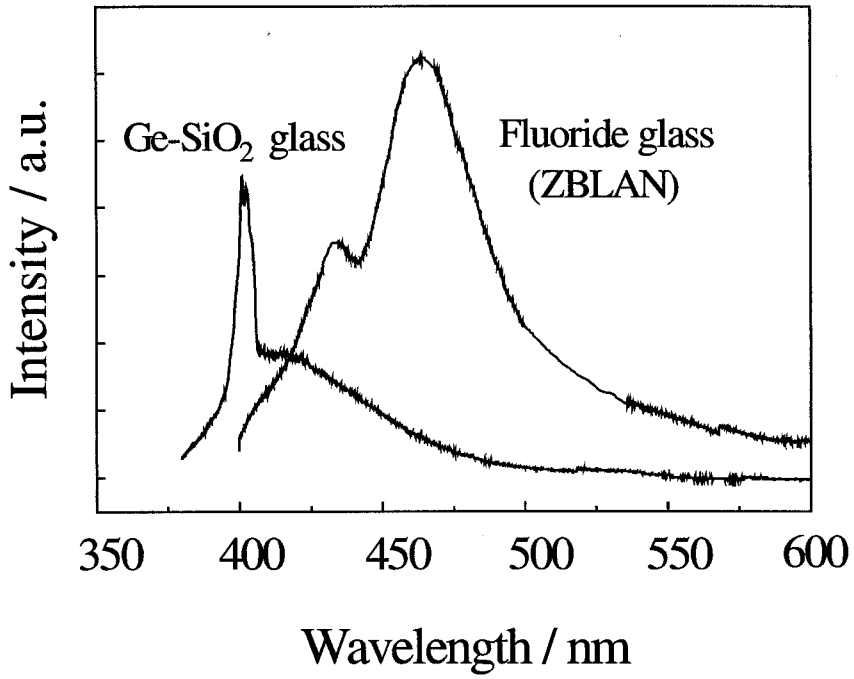

Fig. 1.4. Typical emission spectra of fluoride glass and Ge-doped silica glass during irradiation from an ultrashort-pulse laser. Wavelength, average power and pulse width of the laser were 800 nm, 200 mW and 120 fs at 200 kHz, respectively.

1.1.3.2 Magnitude of the refractive index change

For all translation speeds and directions, structural changes were induced along the path traversed by the focal point of the laser, and colorless, transparent linear damage marks were produced inside every glass that was probed. These damage lines and their cross sections are visible when transmitted light optical microscopy is used and were stable at room temperature. For the high-silica glasses, the damage lines produced when the samples were translated parallel to the axis of the laser beam were roughly cylindrical, with diameters of approximately 12 to 5 μm for the 5-20× microscope objectives. The cross sections of the lines created when the samples were translated perpendicular to the laser axis were elliptical because of the depths of focus of the lenses, and the long dimension of the cross sections ranged from approximately 275 to 100 μm for the 5-20× lenses. For the high-silica glasses, the size of the damage was fairly constant with changing translation speeds. For the soda lime silicate, ZBLAN, and borate glasses, however, the dimensions of the damage area changed significantly with translation speed, and when these glasses were held motionless in the laser beam the damage spread radially from the focal point of the laser with time as if the glass were being slowly melted.

Because of the potential telecommunications applications for the pure and the Ge-doped silica glasses, the properties of the damage in these glasses were examined first. Using a microellipsometer, we measured refractive-index profiles across the cross sections of damage lines that were formed perpendicular to the laser beam. For the pure and the Ge-doped silica glasses, a single pass of the laser produced refractive-index increases of approximately 0.015 and 0.01, respectively, at the center of the damage region (Fig. 1.5). After 10 passes of the laser,

the refractive index at the center of the damage was ~ 0.035 higher than that of the surrounding glass in the Ge-doped silica. The refractive indices of the as-received glasses vary by less than ±0.0005 across the probed region according to the manufacturers' specifications, and the error in the ellipsometer measurements is less than ±0.01. Thus the refractive-index increase in curve (A) of Fig. 1.5, at least, is unquestionably real.

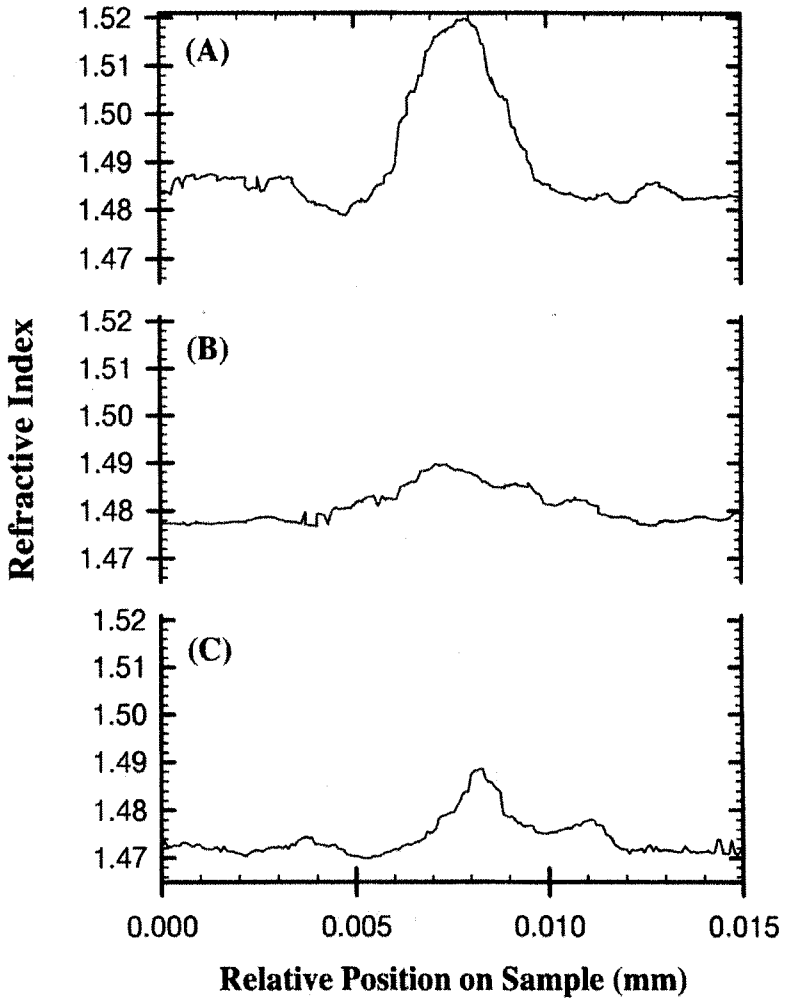

Fig. 1.5. Refractive-index mappings across the cross sections of damage lines created by translation of the samples perpendicular to the laser beam [see Fig. 1(C)] with a 10× lens, an average laser power of 470 mW, and a sample translation rate of 100 μm/s for (A) $3GeO_2$ $97SiO_2$ after 10 passes of the laser along an identical route, (B) $3GeO_2$ $97SiO_2$ after a single pass of the laser, and (C) pure silica after a single pass of the laser. The visible dimensions of the damage cross sections are approximately 6 μm × 180 μm for all the damage marks, so the outer limits of the mappings represent the refractive index of thesurrounding glass.

1.1.3.3 Formation of several defects after laser irradiation

According to ESR measurements (Fig. 1.6), the pure and the Ge-doped silica glasses showed increases in the concentrations of Si E' and Ge E' centers, respectively, and the formation of peroxy radicals and nonbridging oxygen hole centers was observed in both glasses. The UV difference spectra (Fig. 1.7) are in agreement with these assignments [2 - 4] but also show a possible decrease in the concentration of neutral-oxygen monovacancies (NOMV's) in the Ge-doped glass[5]. In addition, unidentified broad absorption bands running from 320 to 700 nm are formed in both glasses.

The creation of defects in the high-silica glasses by 810-nm radiation suggests that the damage mechanism involves a multiphoton process. To our knowledge, such damage at this wavelength has not been reported, and it is suspected that the high pulse energy of the femtosecond laser is responsible for the effect. The photo-induced refractive-index increase in pure-silica glass also appears to be a new observation.

Traditionally it has been suggested that the refractive-index increase resulting from UV irradiation of Ge-doped silica glasses arises from the bleaching of the NOMV band at 5.06 eV (245 nm) owing to the reaction of these sites to form Ge E' centers. More recently, however, it was shown that this bleaching mechanism can account for only a small portion of the refractive-index changes,[6] and a model based on densification and strain in the glass has been proposed [7]. The observed refractive-index increases in both Ge-doped and pure-silica glasses support the idea that the changes are not caused primarily by the NOMV bleaching mechanism, as no NOMV's are found in the UV spectrum of the pure silica. From microscopic observation of the damage region

during irradiation, the structural changes appear similar to what might be expected for localized melting, and it is suspected that the local structural rearrangement is significant. However, we do not yet have direct evidence of densification. It is also not known whether true melting and rapid quenching are occurring, whether the glass is experiencing a combination of defect formation and structural relaxation toward metastable equilibrium, or whether the structural changes are of a different nature. In addition, it is unclear what effect the unidentified absorption bands in Fig. 1.7 have on the refractive index. The refractive-index increases observed here for the high-silica glasses are large enough for the creation of optical devices and waveguides in bulk glasses, and the ability to restrict the refractive-index changes to the region scanned by the focal point of the laser allows one to write complex, three-dimensional patterns in the glass. Writing damage lines perpendicular to the incident light beam provides the most flexibility for writing planar patterns and allows one to create multiple pattern layers by simply changing the focus depth of the beam. Although the lines written perpendicular to the laser are elliptical, it should be possible for one to produce cylindrical damage lines that can serve as light conduits by varying parameters such as the aperture of the microscope lens, the laser wavelength, and the sample thermal history.

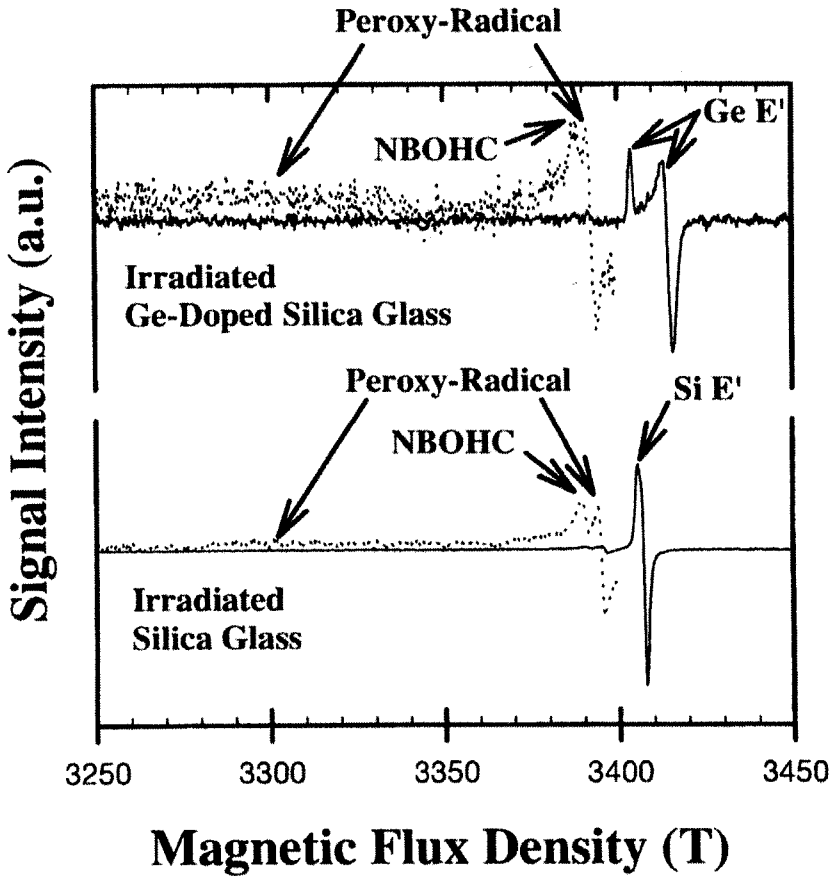

Fig. 1.6. ESR spectra of SiO_2 and $3GeO_2$ $97SiO_2$ glasses after laser irradiation. The solid and the dotted curves indicate ESR spectra collected with 1- and 50-mW microwave powers, respectively. The as-received pure-silica glass contained immeasurably small defect concentrations, and the as-received Ge-doped silica glass contained minute concentrations of ESR-detectable defects compared with the damaged glass. NBOHC's, Nonbridging oxygen hole centers.

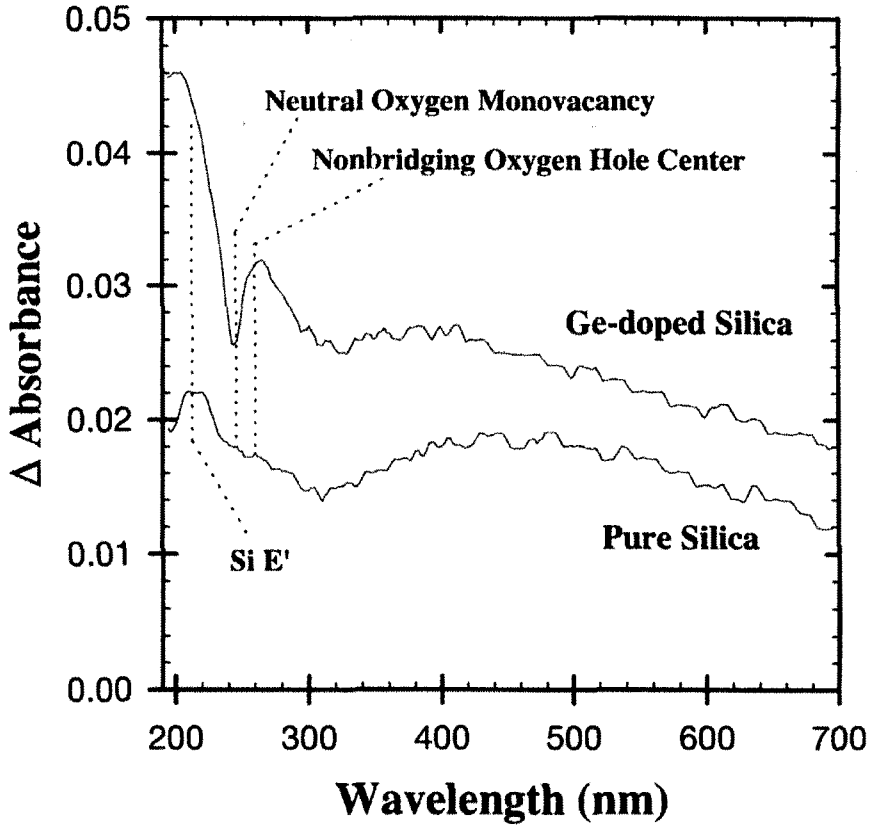

Fig. 1.7. UV difference spectra of the high-silica glasses before and after they were laser irradiated. The Ge-doped silica spectrum is vertically offset by +0.01 for clarity. The noise in these spectra is due to the damaged region, which comprises less than 5 vol.% of the glass probed by the spectrometer beam.

1.1.4 Conclusion

The ability to create photoinduced refractive-index changes in glass by focused, femtosecond laser irradiation at sub-UV wavelengths has been demonstrated. This is important because it is easy to design optical systems that can manipulate this low-photon-energy light without causing laser damage except at the desired focal point of the beam. Moreover, it was possible to create visible but transparent laser damage without cracks in every glass examined. With improvements in the shape of the damage, damage lines formed by this process may one day be used as waveguides in optical circuits.

1.2 Mechamisms of photo-refractive index changes with femtosecond laser pulses

1.2.1 Introduction

The phenomenon of the refractive index change in SiO_2 glass due to ultraviolet (UV) light irradiation has recently gained great interest among glass researchers. It is well-known that Bragg grating writing onto a GeO_2-doped silica optical fiber using refractive index change is induced by UV light irradiation and so on[8,9]. Recently, it has become clear that this refractive index change can also be induced by focusing an ultra-short pulse laser beam [10,11] at a wavelength that cannot be absorbed in one photon process. This is done through a microscope objective and it has become evident that a permanent refractive index change can be induced on 10^{-2}~10^{-3} order on the inside of the SiO_2 glass. With the ultraviolet irradiation, it is difficult to selectively make a high refractive index of only the glass inside. This is because the 5eV-absorption band, which originates from the oxygen defect in the glass, is directly excited by the one-photon process. Furthermore, it has also been confirmed that an increase in the refractive index can be induced in 10^{-2} order in both the Ge-doped and pure SiO_2 glass. However, the mechanism of whether the refractive index change is induced by the ultra-short pulse laser is still unknown. The reason it is difficult to measure this phenomenon is that the refractive index change is limited to the microscopic region.

Confocal microscopic Raman spectroscopy is a powerful tool in this case, because it has a high space resolution and sensitivity to structural change. The purpose of this paper is to investigate the confocal microscopic Raman scattering for the photo-induced refractive

index change found in SiO_2 glass and to reveal the mechanism behind this phenomenon.

1.2.2 Experimental procedure

An experimental apparatus for inducing a high refractive index region in glass has been described elsewhere (see Fig. 1.1). The apparatus used 120fs laser pulses, 800nm in wavelength and 200kHz, that were generated by a laser system comprising a mode-locked Ti:sapphire laser and a regenerative amplifier. A specimen of pure SiO_2 glass with a thickness of about 1mm was translated through irradiating a laser that was focused by a 10X-microscope objective. The refractive index changes were induced along the path traversed by the focal point, and the damege lines were induced inside the SiO_2 glass.

A schematic of an experimental setup for measuring confocal microscopic Raman spectra is shown in Fig. 1.8. To probe the Raman scattering, a sample with a high refractive index region was attached to a holder that could move precisely. The cw laser (Uniphase μ-green laser, 532nm, 50mW) was focused through the spatial filter (pinhole) to make a sample with a 20X microscope objective. In order to measure the Raman spectra, the scattered light focused using the same objective was led by the beam splitter to the entrance slit of the single polychromator (Spex 270M). This was done with a holographic notch filter that could reject strong Rayleigh scattering light and was detected using an intensified charge coupled detector (Princeton ICCD). In order to remove light from the non-focal position of the scattered light, a spatial filter was put on the confocal position.

For a Ge-doped silica glass, to obtain information about the densification with structural change in laser irradiation region, we

observed a non-polishing surface of a core end on a waveguide with an AFM (atomic force microscope). On the surface of the glass used in this observation, it was confirmed that the ablation by laser irradiation was not occurred, in advance.

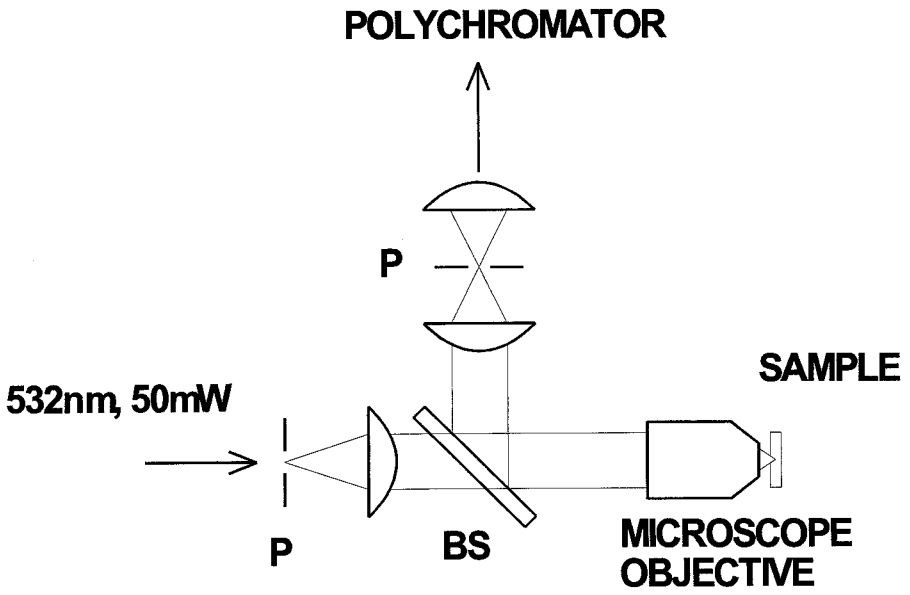

Fig. 1.8. Schematic of the experimental setup. BS: beam splitter; P: pinhole.

1.2.3 Results

First, it was necessary to confirm whether the space resolution of the equipment was sufficient. For this purpose, a sample described some waveguides in the 25 μm interval was prepared. Then, the Raman spectra were measured for two cases: both focused and non-focused on the waveguide. The results are shown in Fig 1.9. There are a lot of noises in this measurement since the exposure time is too short, but from these results, it is clear that we can obtain a Raman spectrum that is in proportion to the existing reproducible waveguide. Thus in place of the waveguide, the features emphasizing the 490-cm^{-1} D_1 band were reproduced. Using these results, the Raman spectra were measured by exposing the features for hours.

Figure 1.10 shows the Raman scattering spectra of the unirradiated region (a) and the waveguide region (b) in SiO_2 glass. In order to evaluate the ω_1 band center value, we show the reduced Raman scattering spectra according to reference 6. The reduced Raman spectra, I_{red} are calculated from the direct spectra $I(\omega_L, \omega_S)$ according to

$$I_{red}(\omega) \equiv \frac{I(\omega_L, \omega_S)}{(\omega_L - \omega)^4} \frac{\omega}{n(\omega)+1},$$

where ω_L is the frequency of the incident laser light, and $\omega_S \equiv \omega_L - \omega$ is the frequency of the scattered light. Thus, ω is the phonon frequency, while $-\omega$ is the Raman shift for the Stokes spectrum. Here,

$$n(\omega) \equiv \frac{1}{\exp(\eta\omega / k_B T) - 1}$$

is the Bose-Einstein occupation number for the sample temperature. In both spectra in Fig.1.10, the features of the pure SiO_2 glass spectrum are evident, including a shoulder near the 490-cm^{-1} D_1 band. The broad band around 430cm^{-1} is attributed to V_S (Si-O-Si), the symmetrical stretching

vibration mode, and is called the ω_1 band. It is clear that the ω_1 band of the high refractive index region has shifted to the high-energy side and narrowed. In contrast, the intensity of the D_1 line has increased slightly. The D_1 line has been interpreted by Galeener [Galeenar 1983] to correspond to the symmetric stretching vibration of oxygen in a tetrasiloxane ring structure. Thus, it is evident that the fourfold planner ring defect increased by the ultrashort laser pulse irradiation.

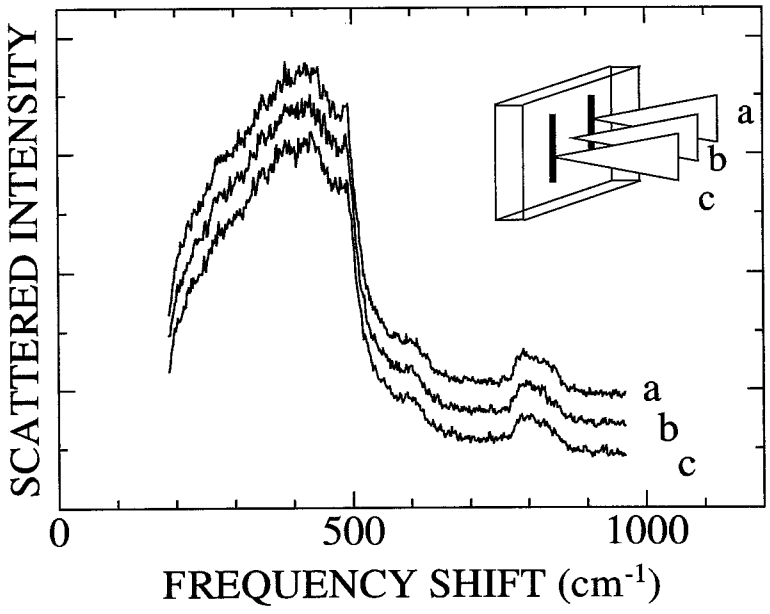

Fig. 1.9. Confocal microscopic Raman spectra in SiO_2 glass described some damage lines in the 25 μm interval induced by ultra-short pulse laser.

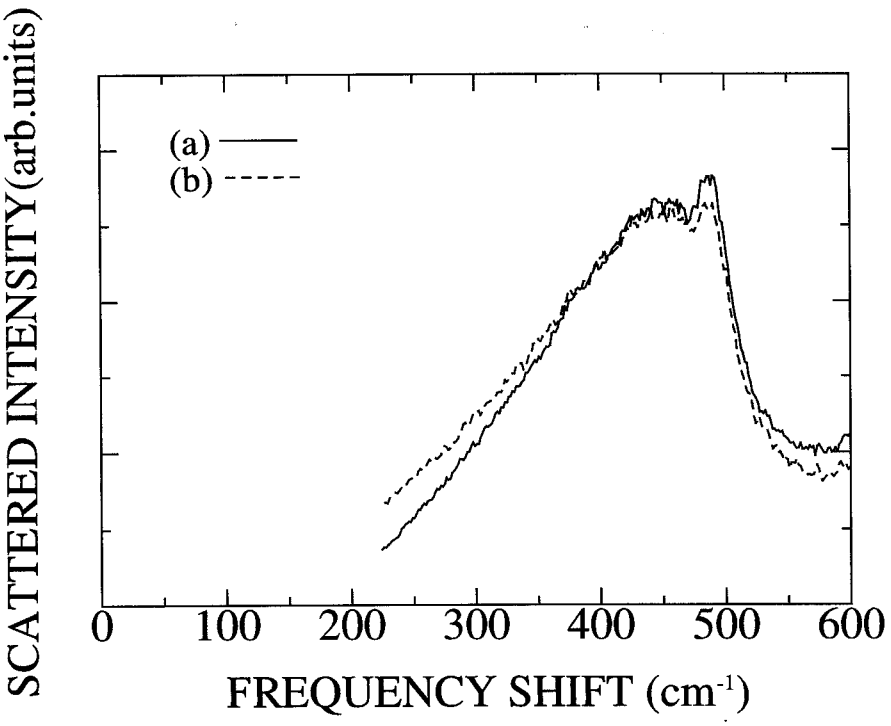

Fig. 1.10. Confocal microscopic reduced Raman scattering spectra of unirradiated region (a) and waveguide region (b) in SiO_2 glass.

1.2.4 Discussion

First, the energy shift of the ω_1 band is discussed. In this study, the shift quantity of the ω_1 band in the high refractive index region was found to be 3~5cm^{-1}. In order to show the relationship between the density and the Raman spectrum of SiO_2 glass, the Raman spectrum of the densified SiO_2 glass was measured. By applying hydrostatic pressure, we found its density is 10% greater than ordinary glass. The results are shown in Fig 1.11. These results proved that the ω_1 band shifts to the high energy side when densifyied and that the energy position of the D_1 band does not shift. Previously, Devine defined the frequency data for the lattice vibrations for the SiO_2 glass [12] that has various densities. From those results, it was found that the ω_1 band of the SiO_2 glass shifts in proportion to the density. Thus the shift of about 4% in the ω_1 band seems to correspond to the increase in density of about 1%.

The relationship between density and the refractive index of the material is known as the Lorentz-Lorenz formula [13] such that:

$$\frac{n^2+1}{n^2+2}\frac{M}{\rho}=\frac{4\pi N\alpha}{3},$$

where M is the molecular weight and $N\alpha$ is the molar polarizability. The refractive index increment of about 0.3% of the SiO_2 glass is corresponds to the density increment of 1%. Though on the sample used in this study, a detailed refractive index was not done, previous measurement results show it is equivalent to the expected refractive index increment, when the laser irradiation condition is considered. This fact indicates the refractive index generates the densification through ultra-short pulse laser irradiation and that a high refractive index occurs.

Fig. 1.12 shows the AFM (atomic force microscope) image of the surface of a core end on silica glass. The shrinkage of the surface

gradually increases from outside the core towards the center and it reaches a maximum at 45 nm. This suggests that densification of a glass occurs in the laser irradiated region. Their research showed that volume increases in the region that generated the refractive index increment, which is consistent with the result of Raman spectra. Although in a photo-induced, high-refractive index region a defect that can not be detected by Raman scattering may also be formed, there is also some possibility of a refractive index change in the local electronic polarizability. Furthermore, this can be seen in the shape of the ω_1 Raman band. The ω_1 band is width originates from the variation of the bond angle between the Si-Os, and is caused by the reflecting features of the amorphous.

According to the simplified central force model, the relation of ω_1 and the bond angle θ of Si-O is established such that $\omega_1^2 = (\alpha / m_0)(1+\cos\theta)$. The ω_1 band spectrum of Fig. 1.11(b) shows that the low-energy side is low-lying compared to the non-laser irradiation region and that the bond angle between Si and O makes this fact into a narrow angle in the laser irradiation region.

Next, we discuss the increase in the intensity of the D_1 line. The D_1 line is a vibration that originates from the symmetrical motion of the oxygen that is localized in the fourfold ring structure. This is clear based on the results of the Raman spectrum found by using the isotope substitution of Galeener et al. [14]. These rings are illustrated in Fig. 1.13. Recently, through using *ab initio* approach to study cluster calculation Uchino *et al* [15]. found that when silica glass is cooled rapidly from a thermal excitation condition, a three- and four-fold ring structure (which is a local stable structure) is formed. Furthermore, they also suggested that the formation of such a local structure prevents atom rearrangement in the cooperative crystallization process. It is possible

that ultra-short pulse laser irradiation can also used to reconstitute an atomic arrangement and that the local stable structure remains like that of a quenching cycle. Actually, a detailed research of the femtosecond time-resolved spectroscopy using laser irradiation is necessary by to determine whether high densification arises. Although there is no proof yet ,atomic rearrangement may occur because of the electronic excitation and/or thermal excitation that causes the Si-O bond angle to narrow and the ring defects to freeze.

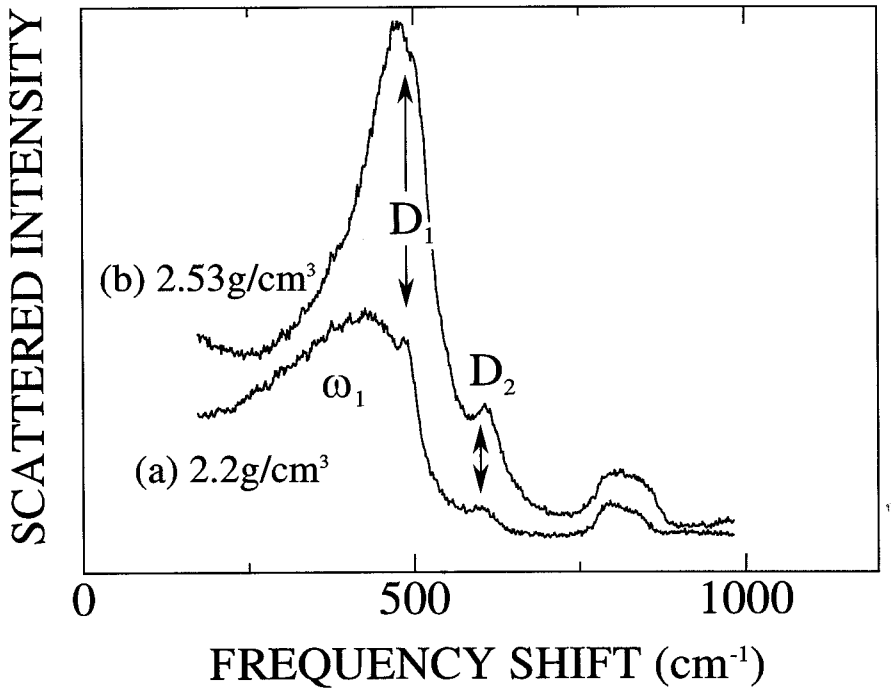

Fig. 1.11. Raman scattering spectra (a) in ordinary SiO_2 glass and (b) densified SiO_2 glass.

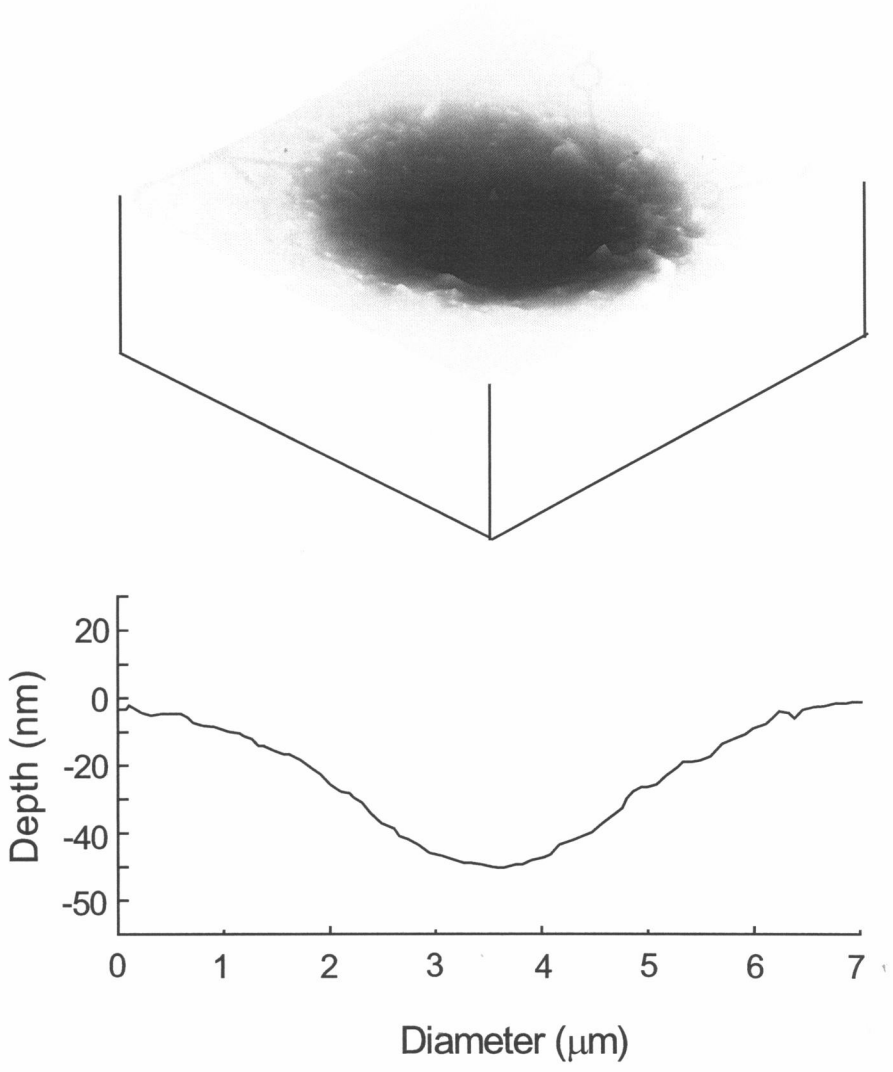

Fig. 1.12. AFM observation of core end surface on silica glass after laser irradiation.

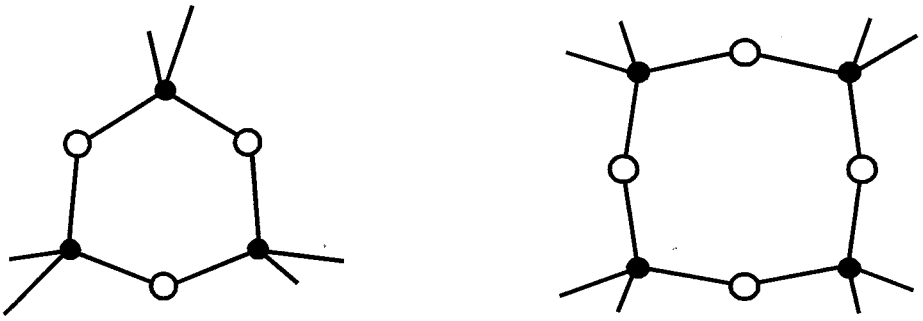

Fig. 1.13 Planar ring structures: (a) threefold ring and (b) fourfold ring. Open circles is oxygen and closed circle is silicon

1.2.5 Conclusions

The confocal microscopic Raman scattering and AFM on the photo-induced refractive index change in SiO_2 glass with an ultra-short pulse laser were measured. We proved that the increase in refractive index caused by the ultra-short pulse laser could be related to the local densification in the glasses. It is also clear that laser irradiation gives the reconstruct ion inside the glass structure.

1.3 Laser-written permanent waveguides in various glasses

1.3.1 Introduction

In section 1.2, it was described that round-elliptical damage lines were written inside various types of glass with femtosecond laser pulses and large increases ($>10^{-2}$) in refractive index were observed in laser-damaged areas induced in germanosilicate glass [10]. Based on these results, we attempted the fabrication of optical waveguides written by a focused ultra-short pulse laser in the femtosecond region. Because of similarities with optical fibers in terms of light guiding and confinement, waveguide structures are very promising in the development of compact, all-solid-state lasers and amplifiers. Most previous methods to fabricate optical glass-waveguides were confined to physical vapor deposition [16] or ionic exchange techniques [17]. Although the waveguides of two-dimensional patterns can be fabricated by these techniques, it is difficult to fabricate three-dimensional waveguides such as those with a spiral structure. To our knowledge, there have been no attempts to form optical glass-waveguides by using photo-induced refractive index change with femtosecond laser pulses. It may be possible to form three-dimensional optical circuits in bulk glasses with such a laserwriting technique.

In this section, the photo-written optical waveguides formed in bulk glasses by a novel method using the focused femtosecond laser were introduced.

1.3.2 Experimental procedure

By using the apparatus shown in Fig. 1, we tightly focused femtosecond laser pulses inside a bulk glass to create localized refractive index changes. Ultra-short pulses (200 kHz, 800 nm) in the Gaussian mode produced by a regeneratively amplified Ti:sapphire laser were utilized to form photo-written waveguides. The pulse width of the laser was continuously adjusted from 110 to 250 fs by changing the dispersive path length of a pair of prisms. The peak energy of the laser pulse at the sample location was approximately controlled between 10 nJ and 5 μW by neutral-density filters that were inserted between the laser and the prism compressor. The laser beam was focused at a diameter of 10 μm or less through microscope objectives and injected into polished samples which included fused and synthetic silica, Ge-doped silica, borosilicate, borate, phosphate, fluorophosphate, fluoride, and chalcogenide glasses. With the help of an XYZ stage controlled by a computer, waveguides were written by translating the sample parallel or perpendicular to the axis of the laser beam (see Fig. 1.14).

For several waveguides written in fluoride glasses, we observed near-field and far-field patterns at several wavelengths ranging from 633 nm to 810 nm. The lights for observation focused via a 50X microscope objective lens were coupled on one end of the core and the intensity distributions for the transmitted lights were measured with a CCD camera. The effects were examined of the average power, the pulse width, and the number of laser passes on the refractive index and on the core size of the optical waveguides.

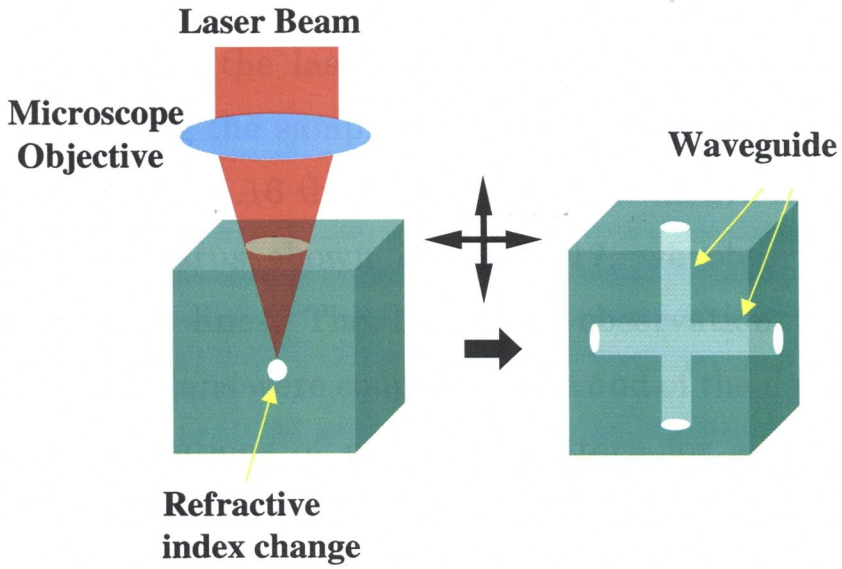

Fig. 1.14. Schematic of optical waveguide writing with high repetition laser pulses.

1.3.3 Results

Using a femtosecond laser with high repetition rate, it is possible to write waveguides, where laser damage spots are continuously induced along a path traversed by the focal point. Waveguides could be written inside various glasses such as fused and synthetic silica, Ge-doped silica, borosilicate, borate, phosphate, fluorophosphate, fluoride, and chalcogenide glasses. Figure 1.15 shows typical photo-written waveguides formed inside synthetic silica, borosilicate, fluoride and chalcogenide glasses with 800 nm, 120 fs, 200 kHz mode-locked pulses

focused through 10X microscope objective. All glass samples were translated at a rate of 20-μm/s. These waveguides were stable at room temperature.

A cross-section of a waveguide written by translating the sample parallel to the axis of the laser beam is shown in Fig. 1.16 (a); that written by translating the sample perpendicular to the axis of the laser beam is shown in Fig. 1.16 (b). Both cross-sections are almost circular. By using the apparatus shown in Fig. 1.17, we observed near-field patterns of damage lines. The lights for observation focused via a microscope objective lens were coupled on one end of the damage line and the intensity distributions of near-field pattern for guided light were measured by a charge coupled device (CCD) camera with the help of a computer. For the damage line in Fig. 1.16 (b), the intensity distributions of a guided light were shown in Fig. 1.18. This result indicated that the damage line function as optical waveguide. When the samples were translated parallel to the laser beam, the shapes of the cross-sections remained unchanged despite changes in the average laser power or the magnification of the objective, with diameters of approximately 7 to 30 μm. The core of the waveguides produced when the samples were translated perpendicular to the laser beam became more elliptical as the numerical aperture was decreased because of the self-focussing. Therefore, a high-numerical-aperture objective should be used to form waveguides with a circular core.

Writing waveguides perpendicular to the incident laser beam provides the most flexibility for writing planer patterns and allows one to create multiple-pattern layers by simply changing the focus depth of the beam (see Fig. 1.19). Figure 1.20 shows the relationship between the pulse width (before through the objective) and internal loss at 1.55 μm for fused silica glass waveguides (straight type) formed perpendicular to

the laser beam, where the core diameters and waveguide length are 8 μm and 50 mm, respectively. The lowest loss was attained when the pulse width of the incident laser pulses is 600fs. A internal loss spectrum measured by cut-back method of the laser induced waveguide which could obtain the lowest loss is shown in Fig. 1.21. The waveguide was formed at a pulse energy of 0.6 μJ, scanning rate of 500 μm/s, repetition rate of 250-kHz and a pulse width of 600fs. Minimum internal loss is 0.1 dB/m or less at near 1.4 μm.

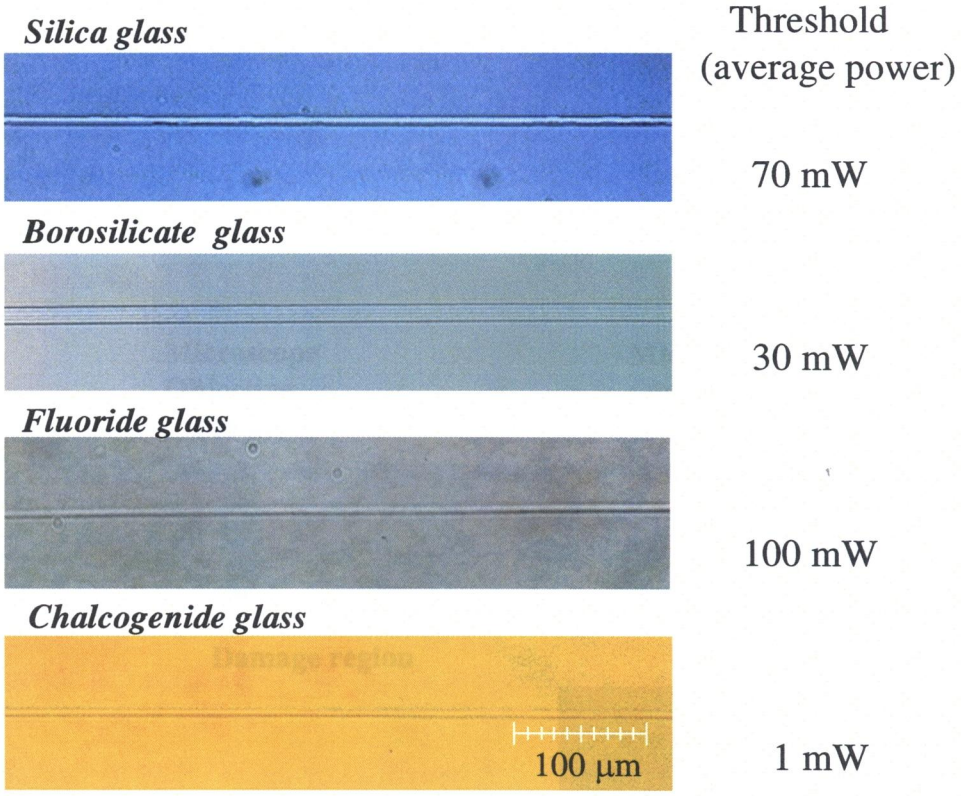

Fig. 1.15. Microscope photograph and writing threshold of photowritten optical waveguides in various glasses.

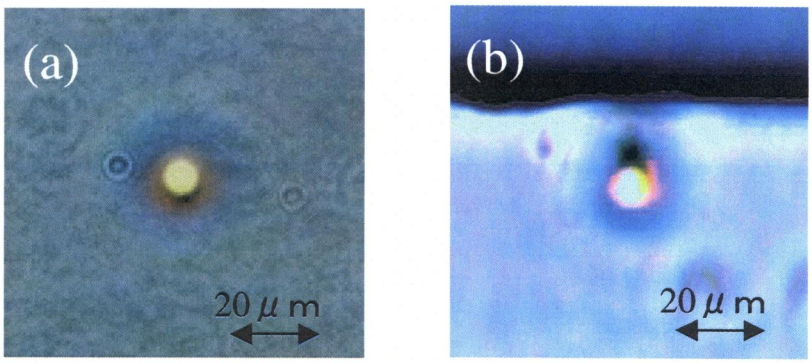

Fig. 1.16. Cross-section of a waveguide written by (a) translating the sample parallel to the axis of the laser beam, and (b) translating the sample perpendicular to the axis of the laser beam.

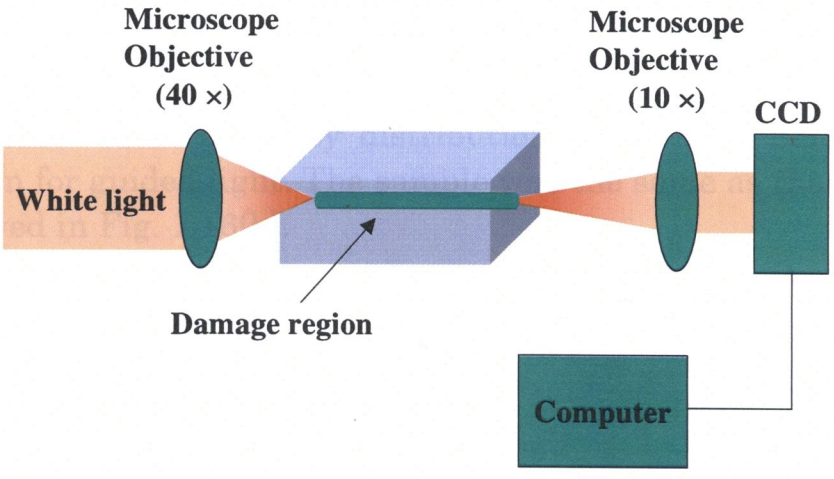

Fig. 1.17. Experimental setup for the intensity distribution measurement of guided light.

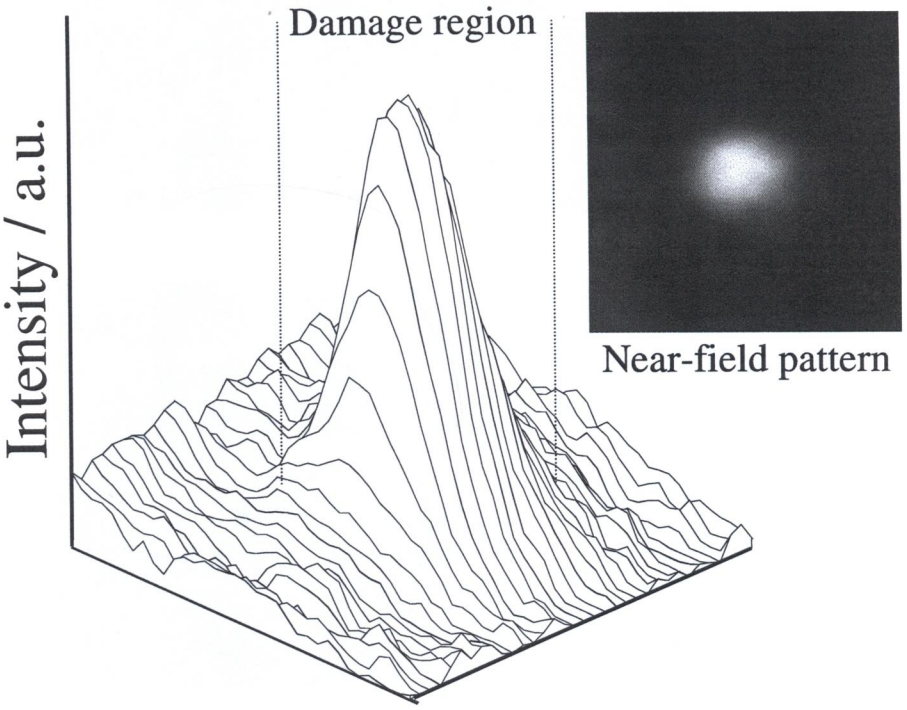

Fig. 1.18. Field intensity distribution of the near-field pattern for guided light. The sample was the same as that observed in Fig. 1.16(b).

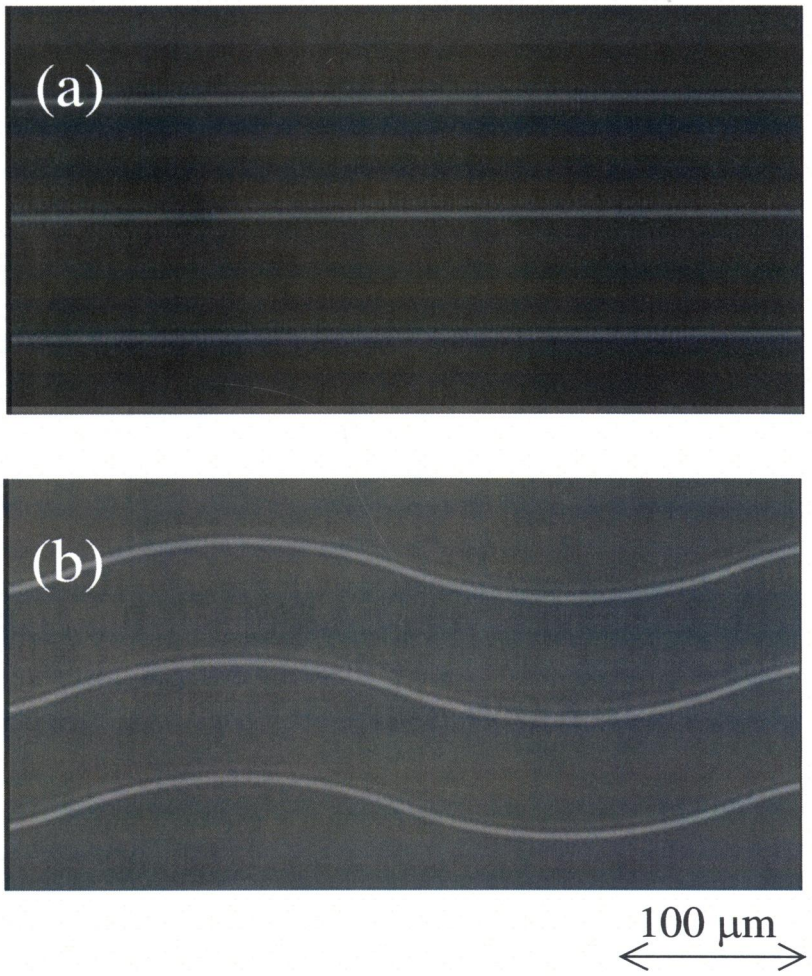

Fig. 1.19. Photo-written waveguides in fluoride glass formed using 800-nm 200-kHz mode-locked pulses. The waveguides were written by translating the sample (a) parallel or (b) perpendicular to the axis of the laser beam at a rate of 20 μm/s and focusing the laser pulses through a 10X or 50X microscope objective, respectively.

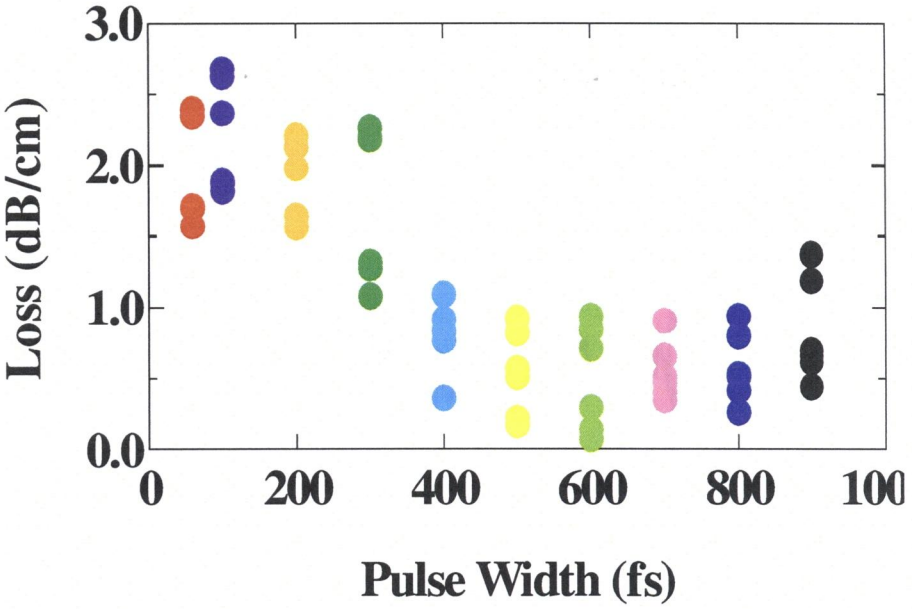

Fig. 1.20. The relationship between the pulse width before through the objective and internal loss at 1.55 μm for fused silica glass waveguides (straight type) formed perpendicular to the laser beam, where the core diameters and waveguide length are 8 μm and 50 mm, respectively.

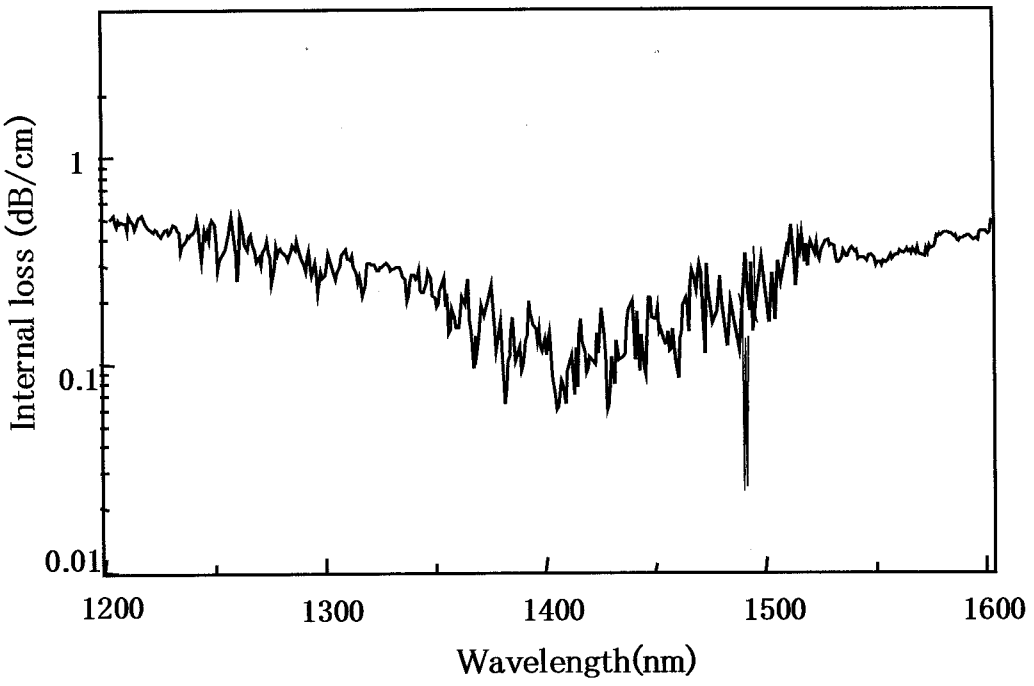

Fig. 1.21. Internal loss of waveguides drawn by translating the silica glass perpendicular to the axis of the laser beam The waveguide was formed at a pulse energy of 0.6 μJ, scanning rate of 500 μm/s, repetition rate of 250-kHz and a pulse width (before through the objective) of 600fs

1.3.4. Discussion

We examined the effects of the average power, the pulse width, and the number of laser passes on the refractive index and core size of optical waveguides. The relationship between the diameter of a core formed by translating the sample parallel to the axis of the laser beam and the average power of the laser is shown in Fig. 1.22. The core diameter increased with the average laser power at a constant pulse width. The intensity profiles of the guided light for waveguides produced at different pulse widths are shown in Fig. 1.23. The peak intensity increased as the pulse width decreased at a constant average power. This shows that the change in the refractive index increases as the pulse width is decreased. That is, the refractive-index change increases with the peak power, which is equal to the average power over the pulse width. Note that the core diameters decreased as the peak power was increased.

As shown in Fig. 1.24, the intensity profiles of the guided light varied with the number of laser passes over the same area. The core diameters remained unchanged despite the number of passes, although increasing the number of passes increased the guided-light intensity due to increasing the refractive index of the core area. These results indicate that the refractive-index difference and the core diameter can be controlled by adjusting the writing conditions.

We observed the field-intensity distributions of the guided light in waveguides written in fluoride glass at different average powers by using a charge coupled device camera. The intensity distributions of the far field at 800 nm for 15-mm-long fluoride-glass waveguides are shown in Figs. 1.25 (a) and (b), where the core diameters were 8 and 27 μm, respectively. At a core diameter of 8 μm, it was possible to propagate only a fundamental mode that was nearly Gaussian, while a complicated

intensity distribution resulting from the overlap of several modes was observed at a core diameter of 27 μm. The cut-off wavelength of the waveguide in Fig. 1.23 (a) was found to be around 800 nm by examining the wavelength dependence of the mode profiles at several wavelengths ranging from 633 nm to 1 μm.

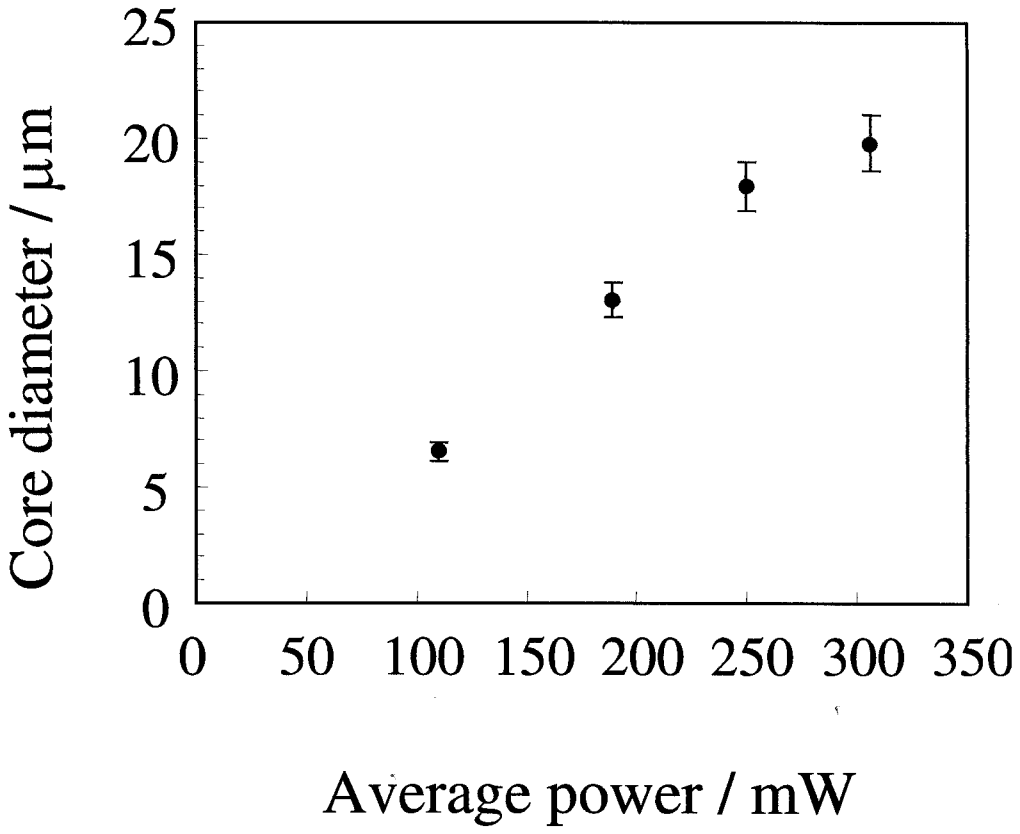

Fig. 1.22. Relationship between the diameter of a core formed by translating the sample parallel to the axis of the laser beam and the average power of the laser. The error bars correspond to the scatter in measured values. Pulse width of the laser was 120 fs.

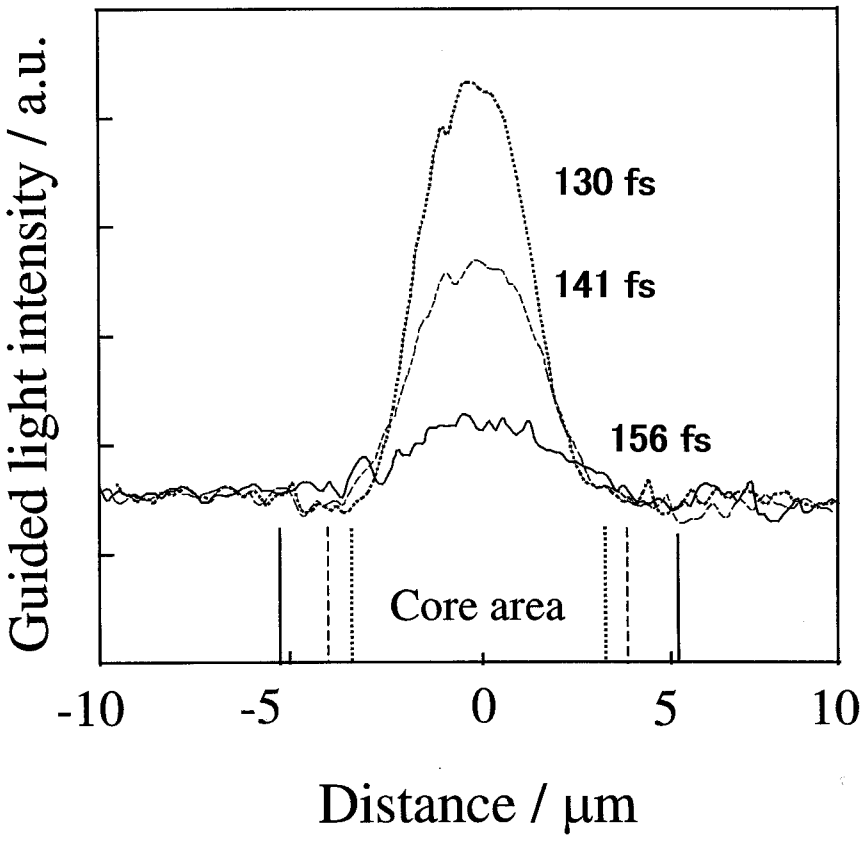

Fig.1.23. Intensity profiles of the guided light for waveguides produced at different pulse widths. Average power of the laser was 150 mW.

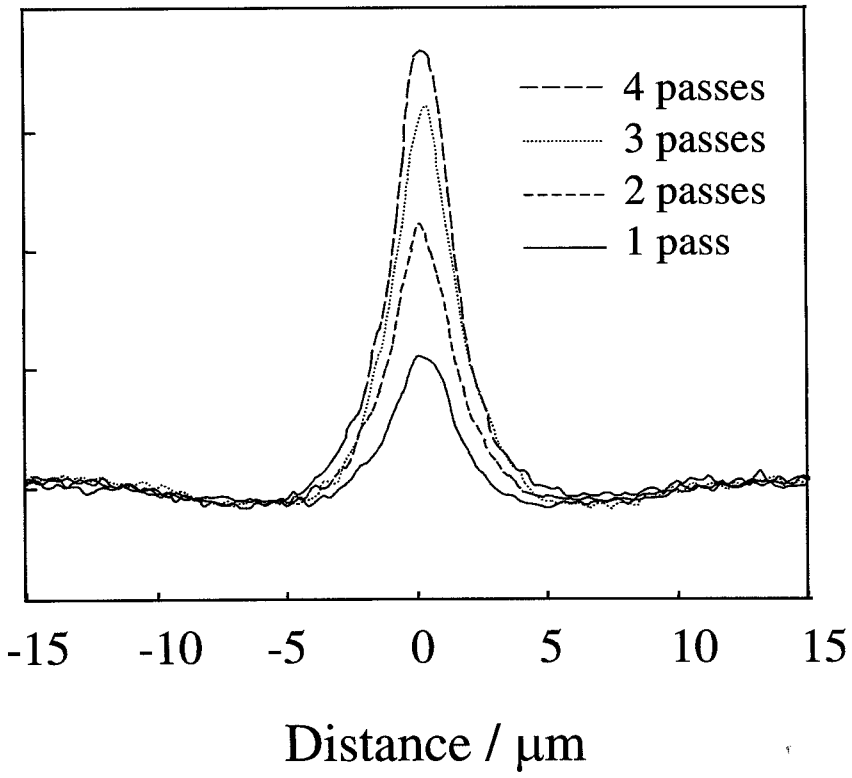

Fig. 1.24. Intensity profiles of the guided light varied with the number of laser passes over the same area. Average power and pulse width were 170 mW and 120 fs, respectively.

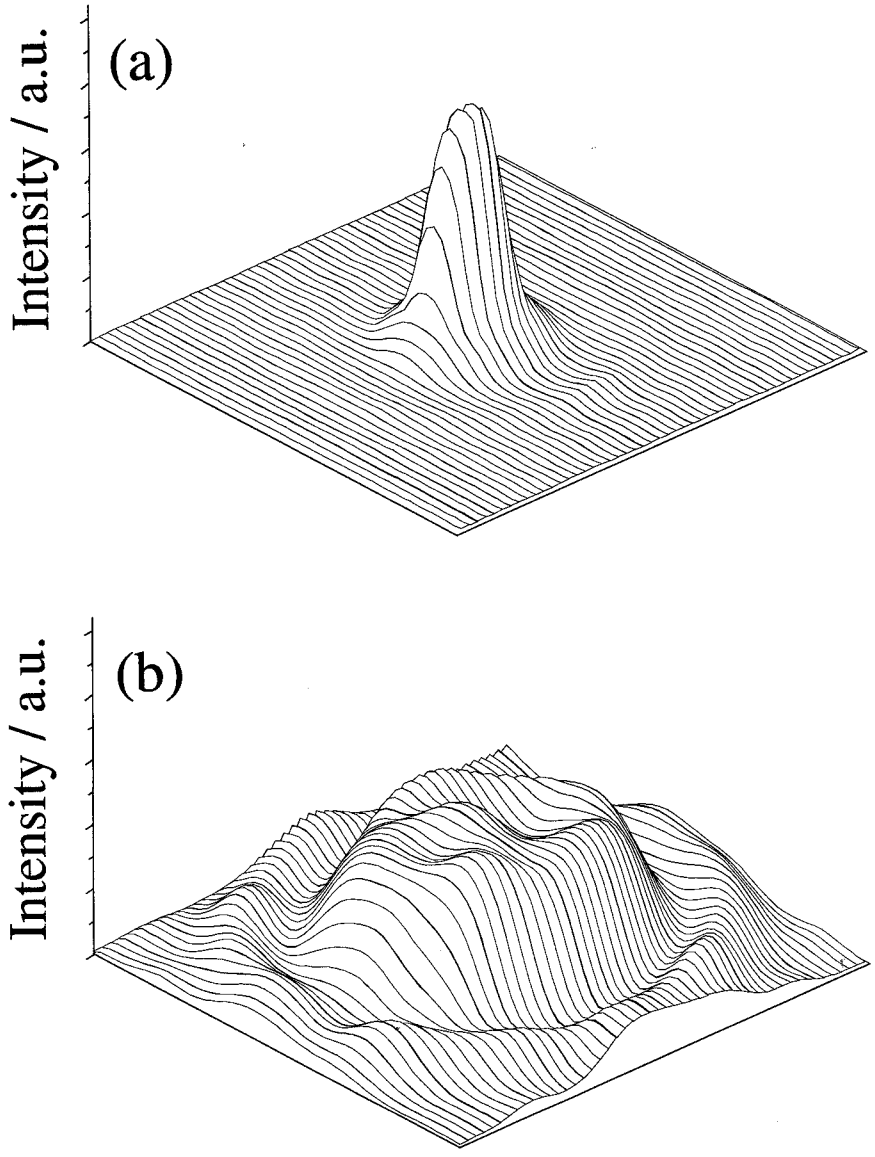

Fig.1.25 Intensity distributions of the far field at 800 nm for 15-mm-long fluoride-glass waveguides where the core diameters were (a) 8μm and (b) 27 μm, respectively.

For the waveguide in Fig. 1.23 (a), on the assumption that the refractive index of the core decreases in proportion to the square of the distance from the center, the result of Hermite-Gaussian fitting for the intensity distributions of the near field is shown in Fig. 1.24. The calculated result is in good agreement with the experimental data, indicating that this waveguide is a graded-index one with a quadratic refractive-index distribution. The refractive indices of the core center and base glass calculated from the result of the fitting were 1.502 and 1.499, respectively.

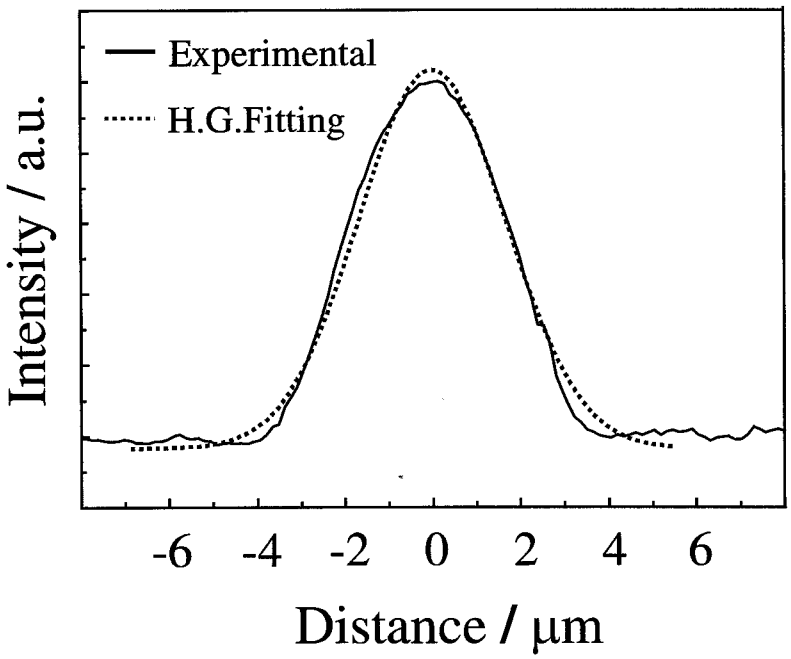

Fig. 1.26. Result of Hermite-Gaussian fitting for the intensity distributions of the near field. The sample was the same as that observed in Fig. 8 (a).

1.3.5 Conclusions

We have shown that optical waveguides can be written in fluoride glass by using a femtosecond laser with a repetition rate of 200 kHz. Examination of the effects of the writing conditions on the refractive index and core size of optical waveguides showed that

- the diameter and refractive index of the core increase with the average laser power at a constant pulse width,
- the refractive index of the core increases and the core diameter decreases as the pulse width is decreased at a constant average laser power, and
- the refractive index of the core increases with the number of laser passes, while the core diameter remains unchanged.

These results mean that the properties of waveguides can be controlled by adjusting the writing conditions.

Our knowledge of the mechanisms behind the permanent change in the refractive index in various glasses is still insufficient. They show that it may be possible to form three-dimensional optical integrated circuits in the interior of same glass compositions by using laser writing.

References

[1] K. O. Hill, Y. Fujii, D. C. Johnson, and B. S. Kawasaki, *Appl. Phys. Lett.* **32**, 647 (1978).

[2] R. A. Weeks and E. Sonder, in *Proceedings of the Symposium on Paramagnetic Resonance* (Academic, NewYork, 1963), Vol. 2, p. 869.

[3] C. M. Nelson and A. R. Weeks, *J. Am. Ceram. Soc.* **43**,396 (1960)

[4] R. A. B. Devine, C. Fiori, and J. Robertson, in *Defects in Glasses*, Galeener F. L., Griscom D. L., and Weber M. J., eds. (Materials Research Society, Pittsburgh, Pa., 1986), p. 177.

[5] R. Tohmon, H. Mizuno, Y. Ohki, K. Sasagane, K. Nagawawa, and Y. Hama, *Phys. Rev.* **B39**, 1337(1989).

[6] D. L. Williams, S. T. Davey, R. Kashyap, J. R. Armitage, and B. J. Ainslie, *Appl. Phys. Lett.* **59**, 762 (1991).

[7] B. Poumellec, P. Niay, M. Douay, and J. F. Bayon , in *Photosensitivity and Quadratic Nonlinearity in Glass Waveguides: Fundamentals and Applications,* (Optical Society of America, Washington, D.C., 1995), Vol. 22, p. 112.

[8] O. K. Hill, B. Malo, F. Bilodeau, C. D. Johnson, and Albert J., *Appl. Phys. Lett.* **62**, 1035 (1993).

[9] E. N. Glezer, M. Milosavljevic, L. Huang, R. J. Finlay, T. H. Her, J. P. Callan, and E. Mazur, *Opt. Lett.* **21**, 2023 (1996).

[10] K. M. Daivis, K. Miura, N. Sugimoto, and K. Hirao, *Opt. Lett.* **21**, 1729 (1996).

[11] K. Miura, J. Qiu, H. Inouye, T. Mitsuyu, and K. Hirao, *Appl. Phys. Lett.* **71**, 3329 (1997).

[12] R. A. B. Devine, *J. Vac. Sci. Technol.* A **6**, 3154 (1988).

[13] M. Born and E. Wolf, *Principles of Optics*, 6th ed. (Pergamon, New York, 1983) p.88

[14] F. L. Galeenar and A. E. Geissberger, *Phys. Rev.* B **27**, 6199 (1983).

[15] T. Uchino and T. Yoko, *Science* **273**, 480 (1996).

[16] E. Paillard, *Proc. EFOC/LAN'87* 108 (1987).

[17] Kawachi, *Workshop Digest '94 Asia-Pacific Microwave Conf.,* 39 (1994).

Chapter 2

Mechanisms and applications of induced structures in rare-earth ions doped glasses by femtosecond laser irradiation

2.1 Long-lasting phosphorescence by the irradiation of femtosecond laser pulses

2.1.1 Introduction

Glass is homogeneous, transparent and can be easily fabricated to various forms such as a flat plate in large size and a fiber. Moreover, a high level of rare earth ions can be "stuffed" into the glass. Therefore, glass is an excellent matrix for rare earth ions to realize various optical functions. So far, the optical properties of glasses doped with trivalent rare earth ions have been investigated intensively, and these glasses have been used as materials for lasers, optical amplifiers and so on [1-3]. However, only a few studies have been performed on the reduced rare earth ions-doped glasses, although glasses containing reduced rare earth ions exhibit various (useful optical properties such as a large Faraday effect, photostimulated luminescence, spectral hole burning memory, etc.[4,5]. The main reason may be that reduced rare earth ions-doped glass must be fabricated under a strong reducing atmosphere. Compared to glasses doped with other reduced rare earth ions, Eu^{2+}-doped glasses are easier to fabricate. Some interesting phenomena in Eu^{2+}-doped glasses have been observed during the past few decades [6,7].

In this part, We introduce three-dimensional long-lasting phosphorescence phenomenon was induced for calcium aluminosilicate

glasses doped with Ce^{3+}, Tb^{3+}, and Pr^{3+} induced by an 800 nm femtosecond pulsed laser. The focused part of the laser in the glasses emits bright and long-lasting phosphorescence able to be clearly seen with the naked eye in the dark even one hour after the removal of the activating laser. By selecting appropriate glass compositions and species of rare earth ions, optional three-dimensional image patterns emitting long-lasting phosphorescence in various colors, including blue, green, and red, can be formed within glass samples by moving the focal point of the laser. The mechanism of the long-lasting phosphorescence is discussed based on absorption spectra of the glasses before and after the femtosecond laser irradiation.

2.1.2 Experimental procedure

The compositions of the glass samples prepared were $40CaO \cdot 30Al_2O_3 \cdot 30SiO_2 \cdot 0.05Ln_2O_3$ (Ln=Ce, Tb, Pr, Nd, Sm, Eu, Dy, Ho, Er, Tm, and Yb) (mol %). Reagent-grade $CaCO_3$, Al_2O_3 , SiO_2 , and rare earth oxides were used as the starting materials. Approximately 30 g batches were mixed and then melted in Pt crucibles at 1550°C for 60 min under an ambient atmosphere. The crucibles containing the melts were then taken out of the furnace, and cooled to room temperature. For the Tb^{3+} -doped glass sample, a part of the obtained glass was pulverized into pieces, put into a glassy carbon crucible, and remelted under an $Ar+H_2$ (5 vol %) atmosphere at 1550 °C for 60 min. The melt was then quenched to room temperature. All of the obtained glasses were transparent. The glass samples were cut, polished, and subjected to optical measurement. The absorption spectra of the samples were measured by a spectrophotometer (JASCO V-570). The normal fluorescence spectra of the samples were measured by a fluorescence spectrophotometer

(Hitachi 850) using 250 nm UV light from a xenon lamp as the excitation source.

A regeneratively amplified 800 nm Ti:sapphire laser was used for our study to emit 120 fs, 200 kHz, mode-locked pulses. The laser beam, with an average power of 400 mW, was focused by a 100 mm focal-length lens on the interior of the glass samples with the help of an *XYZ* stage. For the phosphorescence spectra and decay curves, the glass samples were first irradiated by the focused laser. All of the measurements were carried out at room temperature.

2.1.3 Results and Discussion

After irradiation by the focused laser, no apparent phosphorescence was observed for the Nd^{3+}-, Sm^{3+}-, Eu^{3+}-, Dy^{3+}-, Ho^{3+}-, Er^{3+}-, Tm^{3+}-, and Yb^{3+}-doped glass samples, while visible, bright, and long-lasting phosphorescence from the focused area was observed for the Ce^{3+}-, Tb^{3+}-, and Pr^{3+}-doped glass samples in the dark after the removal of the femtosecond laser. As shown in Fig. 2.1, the emission spectrum of the phosphorescence in the Tb^{3+}-doped glass sample has the same appearance as the photoluminescence spectrum excited by the 250 nm UV light. The emission peaks in the wavelength region from 350 to 600 nm can be ascribed to the $^5D_J \rightarrow {}^7F_{J'}$ (J=3, 4, J'=1-6) transitions of the Tb^{3+} ions. From Fig. 2.1, it is clear that the intensity of the phosphorescence decreases with time, while the appearance of the phosphorescence spectrum remains unchanged.

Figure 2.2 shows the decay curve of the phosphorescence at 437 nm in the glass sample doped with Tb^{3+} ions. The time dependence of the inverse of the intensity of the phosphorescence is also shown in Fig. 2.2. The intensity of the phosphorescence decreases in inverse proportion to

the time, indicating the phosphorescence may be a decay process due to heat-helped tunneling effect.

Figure 2.3 shows a photograph of the emission states of phosphorescence in Ce^{3+} (blue)-, Tb^{3+} (green)-, and Pr^{3+} (red)-doped glasses. The insides of the glass samples were scanned randomly by a focused laser beam moving at a rate of 1000 μm/s. It is surprising that the phosphorescence can still be clearly seen in the dark even one hour after the removal of the activating laser.

The absorption spectra of the Tb^{3+} -doped glass sample before and after laser irradiation were measured and are shown in Fig.2.4. A broad absorption band can be observed peaking at 400 nm in the wavelength region from 280 to 750 nm after the laser irradiation. The band can be ascribed to, for instance, the absorption of aluminum-oxygen hole centers, has been observed for an UV irradiated $CaO\text{-}Al_2O_3$ -based glass sample [8]. The band fading at room temperature shown in Fig. 2.4 agrees with the decay in the phosphorescence. Moreover, the phosphorescence can only be observed in the laser focused area, where color centers were formed after the laser irradiation through observation under a microscope. Therefore, we consider that the disappearance of defects at room temperature is related to the decay of the phosphorescence. The time constant of the phosphorescence was estimated to differ from that of the decay of the absorbance due to laser-induced defect centers. Consequently, phosphorescence and absorption may not be simply related; other factors should be considered.

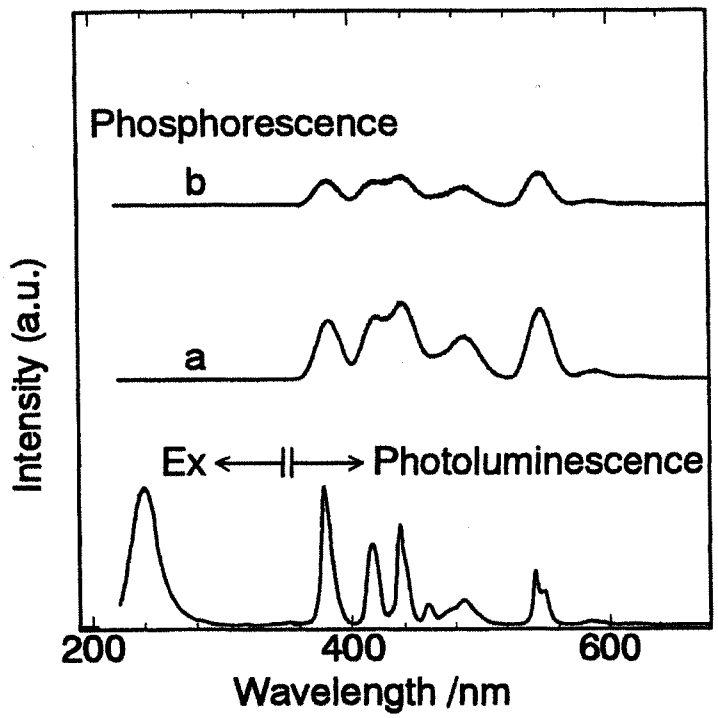

Fig. 2.1. Photoluminescence, phosphorescence, and excitation spectra of a Tb^{3+} -doped calcium aluminosilicate glass. For the measurement of the excitation spectrum, the luminescence at 437 nm was monitored. (a) and (b) are phosphorescence spectra of the glass 350 and 1000 s after the laser irradiation, respectively.

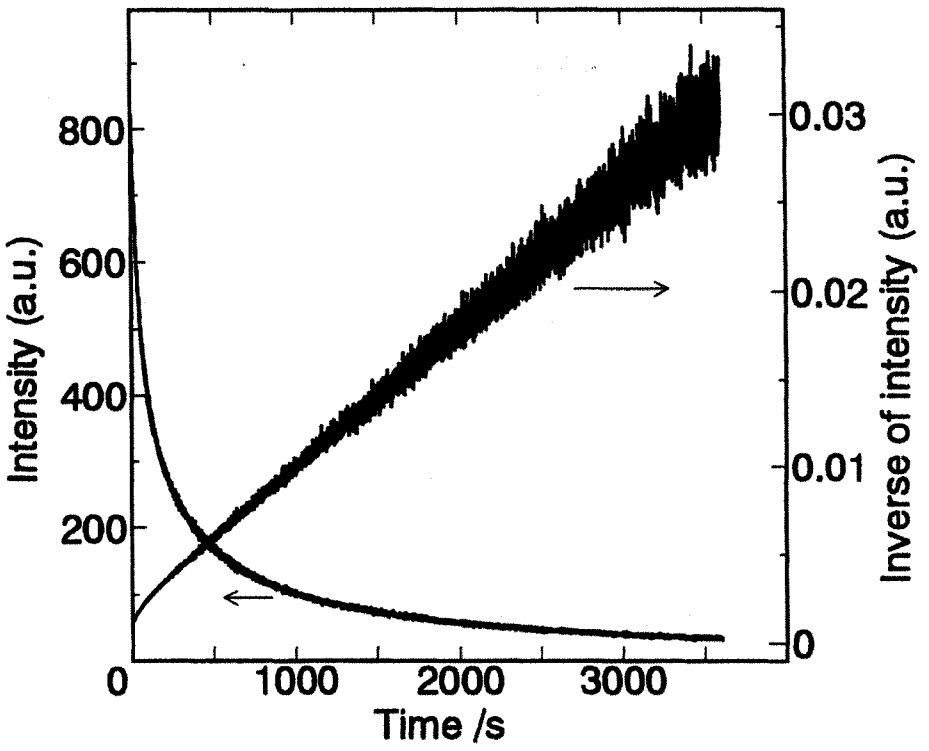

Fig. 2.2. Decay curve of the phosphorescence at 437 nm in a Tb^{3+} -doped calcium aluminosilicate glass.

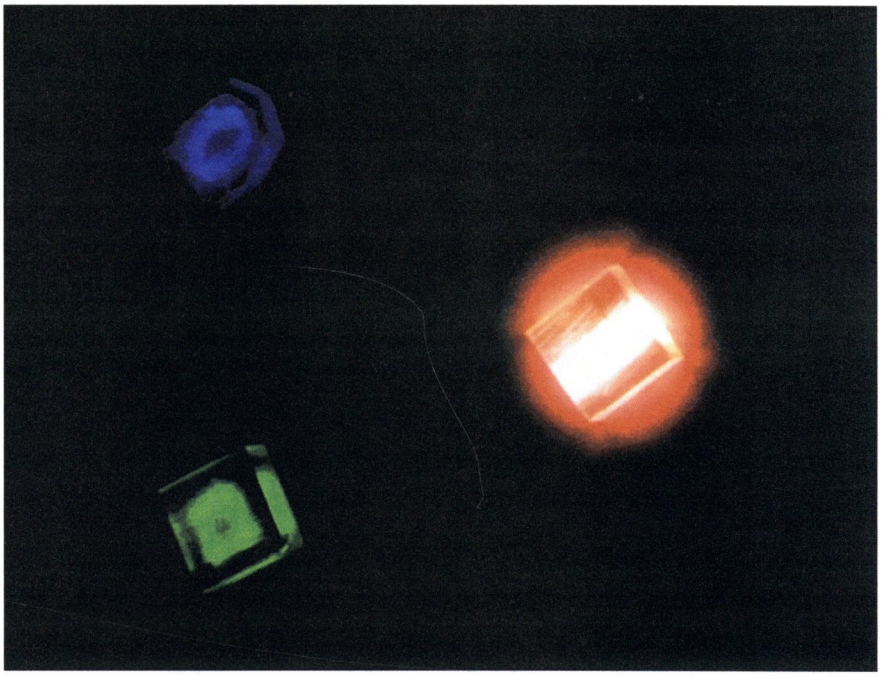

Fig. **2.3.** Photograph of the emission states of phosphorescence in glass samples 5 min after the removal of the exciting laser. The Ce^{3+} -doped calcium aluminosilicate glass sample shows blue light emission. The Tb^{3+} -doped calcium aluminosilicate glass sample shows green light emission. The Pr^{3+} -doped calcium aluminosilicate glass sample shows red light emission.

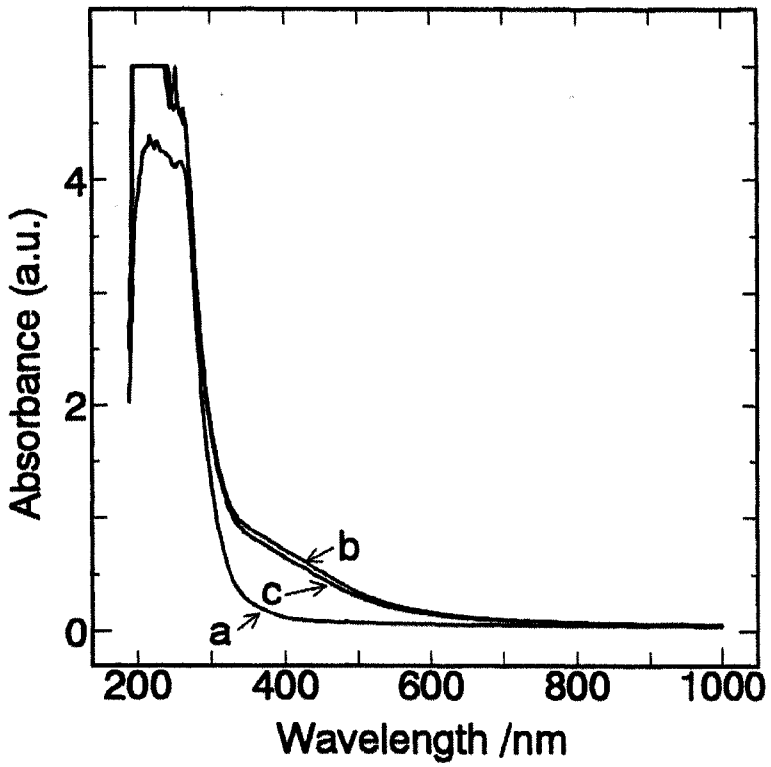

Fig. 2.4. Absorption spectra of a Tb^{3+} -doped calcium aluminosilicate glass before and after the irradiation of a femtosecond laser. (a) Before the laser irradiation. (b) Upon the removal of the femtosecond laser. (c) 30 min after the removal of the femtosecond laser.

Long-lasting phosphorescence phenomenon in the Ce^{3+} -, Tb^{3+} -, and Pr^{3+} -doped glass samples was observed. However, we did not observe the same phenomenon in the other rare earth ion doped glass samples. We therefore suggest that the mechanism of the long-lasting phosphorescence in the glass samples is as follows: Ce, Tb, and Pr are elements that lead to the easy formation of Ln^{4+} (Ln=rare earth) [9]. Since all of the glasses were fabricated under an ambient atmosphere, Ce, Tb, and Pr may have already existed as mixed states of Ln^{3+} and Ln^{4+}. Ln^{3+} can possibly act as hole trapping centers while Ln^{4+} is known to act as electron trapping centers.

The long-lasting phosphorescence phenomenon was observed in the Tb^{3+} -doped glass sample fabricated under a strong reducing atmosphere . This eliminated the possibility of Ln^{4+} acting as electron trapping centers in the present case. After the irradiation by the focused femtosecond pulsed laser, free electrons and holes were formed in the glass samples through multiphoton ionization, Joule heating, and collisional ionization processes [10]. The holes or electrons were trapped by defect centers, released by heat
at room temperature, and recombined with electrons or holes trapped by other defect centers. The released energy, due to the recombination of holes and electrons, was transferred to the rare earth ions and excited the electrons at the ground state to an excited state, leading to the characteristic rare earth ion emissions.

The probability of energy transfer between defects and rare earth ions is proportional to the folded area of absorption, due to the transitions of the ground state and excitation state of the defects and rare earth ions, and is inverse proportion to the distance between the defects and rare earth ions [11]. The released energy may just be in good agreement with the energy level of the rare earth ions in Ce^{3+}-, Tb^{3+}-,

and Pr^{3+} -doped glass samples since the $5d$-$4f$ transition of Ce^{3+}, Tb^{3+}, and Pr^{3+} has a lower energy than those of other rare earth ions. Moreover, the hole or electron trap depth is broadly distributed and shallow, resulting in the occurrence of the long-lasting phosphorescence at room temperature. The detailed mechanism should be investigated further.

2.1.4 Conclusion

In conclusion, we have observed femtosecond infrared laser-induced long-lasting phosphorescence in Ce^{3+}, Tb^{3+}, and Pr^{3+} doped calcium aluminosilicate glasses. The long-lasting phosphorescence is considered to be due to the thermal stimulated recombination of holes and electrons at traps induced by the laser irradiation, which leave holes or electrons in a metastable excited state at room temperature. We suggest that it may be possible to selectively induce defects by using lasers with different wavelengths, pulse widths, and repetition rates. The energy due to the recombination of holes and electrons in various defects may be different and selectively excite the electrons in the ground state to an excited state of rare earth ions, e.g., Pr^{3+} , leading to the occurrence of phosphorescence in various colors in a glass. We think that it may also be possible to induce defects that are stable at room temperature by using an ultra-fast pulse laser and that are able to be released by another laser.

This will be very important in the fabrication of rewritable three-dimensional optical memory devices with both an ultrahigh recording speed and an ultrahigh storage density.

2.2 Permanent photo-reduction of Sm^{3+} to Sm^{2+} inside glasses

2.2.1 Introduction

Reduced rare-earth ion doped glasses exhibit a large Faraday effect, long-lasting phosphorescence, photo-stimulated luminescence, photochemical spectral hole burning memory, and other important properties [12-15]. They are expected to be promising materials in the optoelectronic field.

To obtain a glass doped with reduced rare-earth ions, e.g., Sm^{2+} and Eu^{2+}, the glass must be fabricated under a strong reducing atmoshere [12-15]. Moreover, it is difficult to prepare a glass samples, so that rare-earth ions exist in a reduced state in some small micrometer dimensions inside the glass sample by using an atmosphere-controlling process.

Rare-earth ions in solutions show broad absorption bands and sharp absorption peal in the UV and near-UV to near-IR wavelength regions [16]. The broadband are due to the charge transfer state (CTS) or *5d-4f* transitions of rare-earth ions. The sharp peaks are due to the *4f-4f* inner shell transitions of rare-earth ions. Recently, it was found that direct excitation of the CTS and *5d-4f* transition bands can induced photo-reduction in some rare-earth ions [17,18]. However, such studies concentrated on the photo-reduction of rare-earth ions in solutions.

In this section, the observation of the permanent photo-reduction in some rare-earth ions of Sm^{3+} to Sm^{2+} in a sodium aluminoborate glass by 800 nm femtosecond laser pulses. The mechanism of the phenomenon is also discusses based on the absorption and electron spin resonance (ESR) spectra of the glasses before and after the laser irradiation.

2.2.2 Experimental procedure

The composition of a Sm^{3+} -doped glass sample used in this study was $0.05Sm_2O_3 \cdot 10Na_2O \cdot 5Al_2O_3 \cdot 85B_2O_3$ (mol%). Reagent grade Sm_2O_3, Na_2CO_3, Al_2O_3, and B_2O_3 were used as starting materials. A mixed 30 g batch was melted in a Pt crucible at 1250 °C for 30 min, under an ambient atmosphere. The melt was then poured on a stainless-steel plate, and a transparent and colorless glass sample was obtained. For comparison, Sm^{2+} -doped glass samples with compositions of $0.5Sm_2O_2 \cdot 10Na_2O \cdot 5Al_2O_3 \cdot 85B_2O_3$ and $0.05SmF_2 \cdot 53HfF_4 \cdot 20BaF_2 \cdot 4LaF_3 \cdot 3AlF_3 \cdot 20NaF$ (mol%) were prepared by melting the batches in glassy carbon crucibles under an $Ar+H_2$ (5 mol%) atmosphere at 1250 °C for 60 min, in a horizontal carbon furnace and quenching the melts to room temperature. Transparent, orange glass samples were obtained. After annealing the glass samples at the respective glass transition temperature (Tg) for 1 h, they were cut, polished, and then subjected to optical property measurements.

A regeneratively amplified 800 nm Ti:sapphire laser that emits 120 fs, 200 kHz, mode-locked pulses was used for our study. A laser beam with 400 mW average power was focused using a 10× objective lens with a numerical aperture of 0.30 on the interior of the glass samples with an XYZ stage.

Absorption spectra of the glass samples were measured by a spectrophotometer (JASCO V-570). Photoluminescence spectra of the glass samples were measured by a fluorescence spectrophotometer (SPEX 270M) using 514.5 nm light from an Ar^+ laser as the excitation source. ESR spectra of the glass samples were measured by an ESR spectrophotometer (JEOL-FE3X). All of the experiments were carried out at room temperature.

2.2.3 Results and Discussion

After irradiation by the femtosecond laser, the focused area in the glass sample was orange as observed in an optical microscope. Figure 2.5 shows the absorption spectra of the Sm^{3+} -doped glass sample before (a) and after (b) the femtosecond laser irradiation. Small peaks at 340, 350, 375, 400, and 415 nm and a strong band at 210 nm can be ascribed to the $4f$–$4f$ transitions and CTS of Sm^{3+} [5,9,19]. Absorption in the 200–600 nm region increased after the laser irradiation.

Figure 2.6 shows the differential spectrum (a) between the absorption of the Sm^{3+} -doped glass sample after and before the laser irradiation. For comparison, the absorption spectra of the Sm^{2+} -doped fluorohafnate glass sample (b) and the Sm^{2+} -doped sodium aluminoborate glass sample (c) are also shown. A broadband peaking at approximately 320 nm can be observed in the differential spectrum of absorption. Compared with the absorption spectra of the Sm^{2+} -doped glass samples fabricated under a reducing atmosphere, the broadband in the glass sample after the laser irradiation can be mainly ascribed to the absorption due to the $5d$–$4f$ transitions of Sm^{2+} [5,19].

Figure 2.7 shows the photoluminescence spectra of the Sm^{3+} -doped glass sample before (a) and after (b) the laser irradiation. The emissions at 560, 600, 645, and 705 nm in the unirradiated glass sample can be attributed to the $4f$–$4f$ transitions of Sm^{3+}. The four new peaks at 683, 700, 724, and 760 nm observed in the photoluminescence spectrum of the laser-irradiated glass sample can be attributed to the $4f$–$4f$ transitions of Sm^{2+}. Similar to the results of the absorption spectra, the photoluminescence spectra showed that a part of Sm^{3+} was converted to Sm^{2+} after the laser irradiation. At present, we cannot calculate the exact quantum yield of the reaction due to space resolution limitations in

our photoluminescence measurement system. A precise analysis is being performed.

What exactly is the mechanism of the photoreduction of Sm^{3+} to Sm^{2+} after the femtosecond laser irradiation? The Sm^{3+} -doped glass sample has no absorption in the 700–900 nm region, so the photoreduction of Sm^{3+} to Sm^{2+} should be a multiphoton reduction process. Figure 2.8 shows the ESR spectra of the Sm^{3+} -doped glass sample before (a) and after (b) the laser irradiation. No apparent signals can be observed in the spectrum of a laser-unirradiated glass sample, while strong signals at approximately g=2.0 can be observed in the spectrum of the laser-irradiated glass sample. The signals can be assigned to the defect centers of holes trapped by nonbridging oxygen ions and tetrahedral coordinated boron atoms, and electrons trapped by the quasi-F centers as in γ ray-irradiated sodium borate glasses [20].

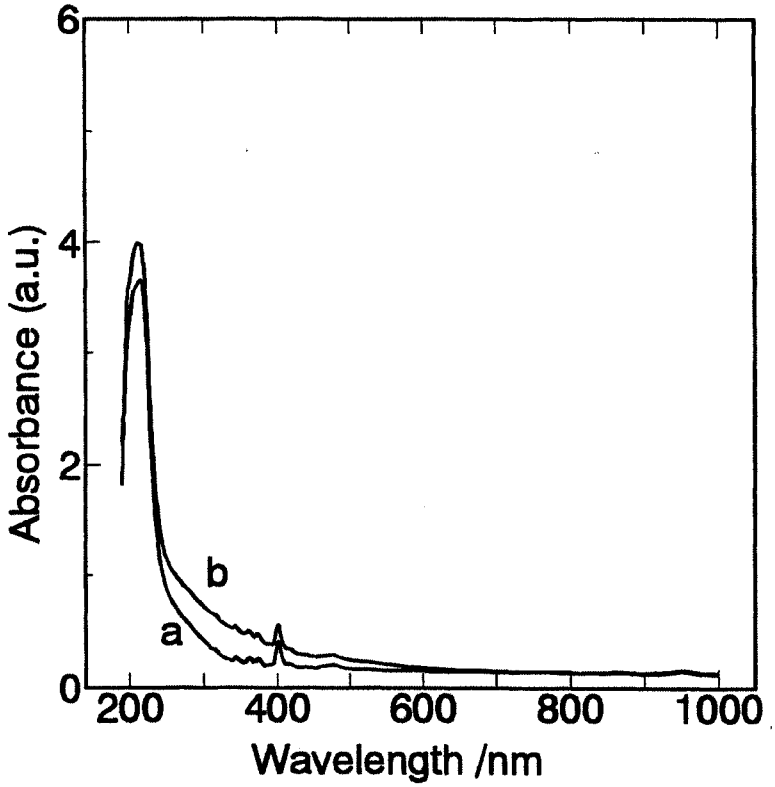

Fig. 2.5. Absorption spectra of Sm^{3+} -doped sodium aluminoborate glass before (a) and after (b) femtosecond laser irradiation.

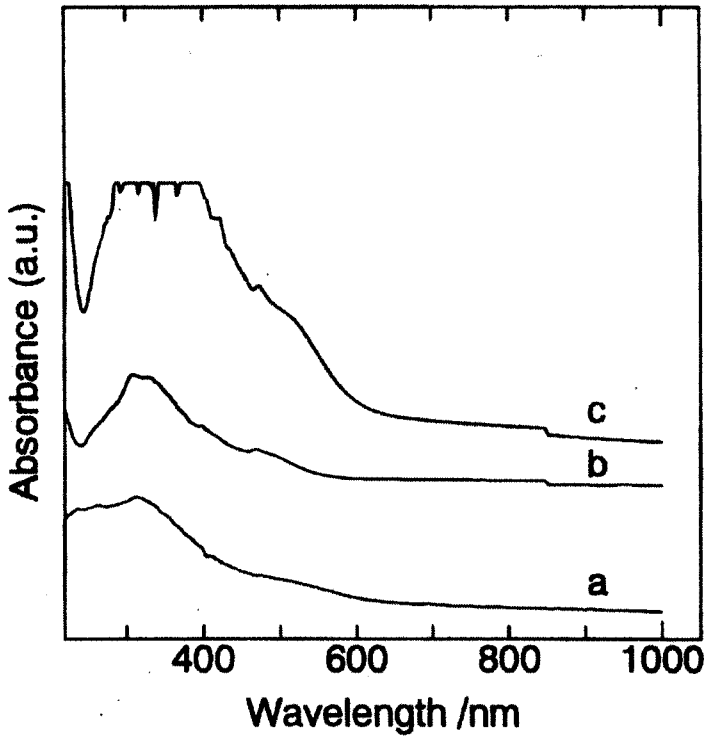

Fig. 2.6. Differential spectrum (a) between absorption of Sm^{3+} -doped sodium aluminoborate glass after and before femtosecond laser irradiation, absorption spectra of Sm^{2+}-doped fluorohafnate (b) and Sm^{2+} -doped sodium aluminoborate (c) glass samples fabricated under reducing atmosphere.

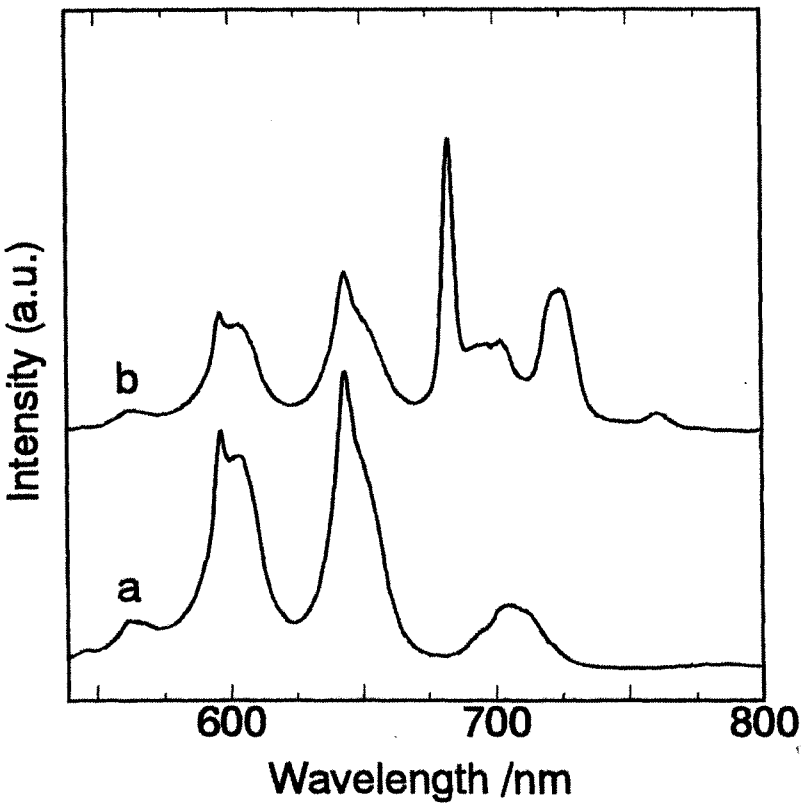

Fig. 2.7. Photoluminescence spectra of Sm^{3+} -doped sodium aluminoborate glass before (a) and after (b) femtosecond laser irradiation (excitation source from Ar^{+} laser at 514.5 nm).

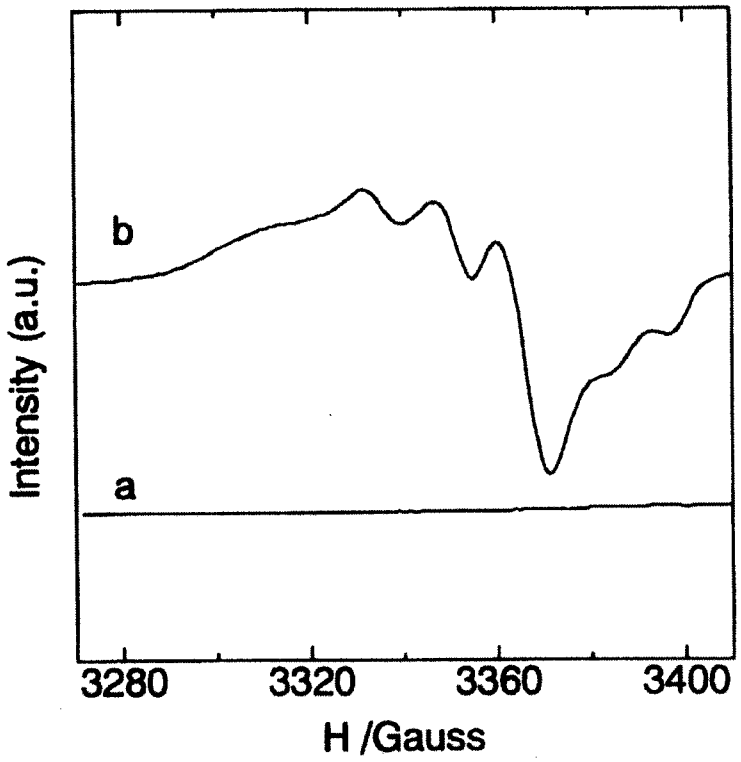

Fig. 2.8. ESR spectra of a Sm^{3+} -doped sodium aluminoborate glass before (a) and after (b) femtosecond laser irradiation.

Although the mechanism is not fully clear at present, we believe the mechanism of photoreduction is as follows. Following the irradiation of the focused femtosecond laser, active electrons and holes were created in the glass through multiphoton ionization, Joule heating, and collisional ionization processes [21]. Holes were trapped by nonbridging oxygen ions as well as by tetrahedral coordinated boron atoms, while some of the electrons were trapped by the Sm^{3+}, which led to the formation of Sm^{2+} . The reactions are expressed as (I) and (II) in Fig. 2.9.

The trap levels of defect centers may be deep, resulting in stable Sm^{2+} at room temperature. We have examined the thermal stability of the photoreduction product, Sm^{2+}. The results showed that Sm^{2+} was stable at room temperature. When the temperature exceeded *Tg*, Sm^{2+} was reconverted to Sm^{3+}, indicating that reverse reactions of I and II occurred at a temperature above *Tg*.

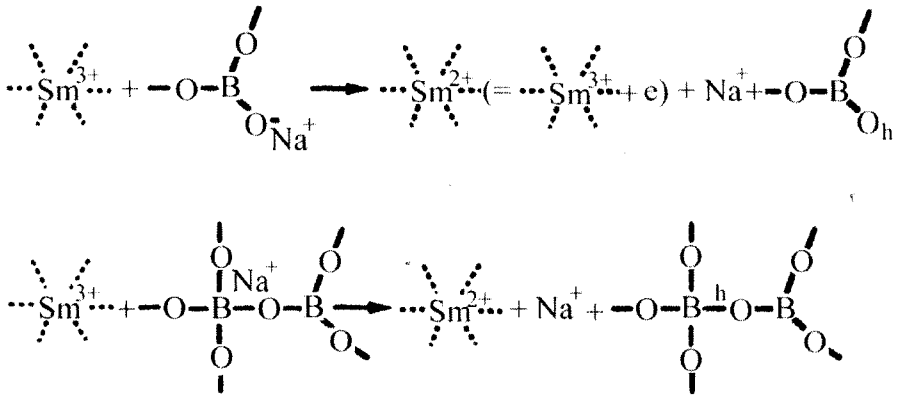

Fig. 2.9. Mechanism of photoreduction of Sm^{3+} to Sm^{2+} in Sm^{3+} -doped sodium aluminoborate glass after femtosecond laser irradiation.

2.2.4 Conclusion

Permanent photoreduction of Sm^{3+} to Sm^{2+} by a focused infrared femtosecond pulsed laser was observed. The results demonstrate the possibility of selectively inducing a change of valence state of Sm^{3+} ions on the micrometer scale inside a glass sample by use of a focused nonresonant femtosecond pulsed laser. Whereas a three-dimensional optical memory has approximately 10^{13} bits/cm^3 storage density, which means that data information can be stored in the form of a change in refractive index in a spot.

An optical memory using a valence-state change of rare-earth ions in a spot may have the same storage density and may allow one to read out data in the form of luminescence, thus providing the advantage of a high signal-to-noise ratio. Therefore, the present technique will be useful in the fabrication of three-dimensional optical memory devices with high storage density.

2.3 Three-dimensional optical memory with rewriteable and ultrahigh density using valence state change of samarium ions

2.3.1 Introduction

Materials processing technology by using femtosecond laser irradiation has attracted tremendous interest from both the scientific and technological communities. In particular, the use of femtosecond laser processing to write three-dimensional (3D) structures in transparent materials is technologically attractive for applications such as multi-layer optical memories[22,23] and optical waveguides(in section 1.3) . 3D optical memories have generated considerable interest in recent years for their potential application to high-density optical data storage[24,25]. Previous researches on 3D optical memories using irradiation with a focused femtosecond laser have demonstrated the use of refractive index changes or void creation in transparent materials [26,27].

In section 2.2, it was found that samarium ions in glass can be space-selectively photoreduced with an infrared femtosecond laser. In this section, we examine the possibility of achieving 3D optical data storage inside glass by using a focused femtosecond laser to permanently photoreduce of Sm^{3+} to Sm^{2+}.

2.3.2 Experimental procedure

The composition of the glass samples doped with samarium ions used in this study was $35AlF_3$-$10BaF_2$-$10SrF_2$-$20CaF_2$-$10MgF_2$-$14.5YF_3$ -$0.5SmF_3$ (mol%). Samarium was present in the glass in the Sm^{3+} ionic state. As a recording source we employed a regeneratively amplified

800-nm Ti:sapphire laser emitting 20-Hz or 250-kHz mode-locked pulses. We tightly focused femtosecond laser pulses inside the bulk glass to locally photoreduce Sm^{3+} to Sm^{2+}. A 3D recording was made by laser irradiation through a water-immersion objective (63X magnification, NA=1.2) in the interior of the glass samples with an XYZ stage. Photoluminescence images were obtained with a three-dimensional nanometer-scanning spectroscopic microscope (-nanofinder TII) using 488-nm light from an Ar^{+} laser as the readout (excitation) source. All experiments were carried out at room temperature.

2.3.3 Results and Discussion

Figure 2.10 shows photoluminescence spectra obtained by excitation at 488 nm for a laser-irradiated area (a) and non-irradiated area (b) in the interior of the glass. Comparing (a) to (b) shows that the emission in the 650-775-nm region differed appreciably. The broad bands observed around 560, 600, and 645 nm can be attributed to the $^4G_{5/2} \rightarrow {}^6H_{5/2,7/2,9/2}$ transitions, respectively, of the Sm^{3+} ions. On the other hand, the emissions at 680, 700, and 725 nm are attributed to the $^5D_0 \rightarrow {}^7F_{0,1,2}$ transitions, respectively, of the Sm^{2+} ions. This means that laser-irradiated areas (photoreduced areas) recorded inside glass can be detected only by emissions at 680, 700, or 725 nm. Although the mechanism is not fully clear at present, we suggest the mechanism of the photoreduction is as follows. Active electrons and holes were created in the glass through multiphoton process. Holes were trapped in the active sites in the glass matrix while some of electrons were trapped by the Sm^{3+}, leading to the formation of hole trapped defect centers and Sm^{2+}.

By using the photoreduction of Sm^{3+} to Sm^{2+}, alphabetical characters were recorded in the form of sub-micron size bits in a

three-dimensional (layered) manner in a glass samples. Here, one recorded character consisted of 300 to 500 photoreduction bits recorded with 5000 laser shots per bit with a repetition rate of 250 kHz. The spacing between alphabetical characters was 2 μm. The bits had a diameter of 400 nm, which was significantly smaller than the focal-beam size and the wavelength of the recording laser. Figure 2.11 shows photoluminescence images of alphabetical characters recorded on different layers, which were observed by using a 40X objective lens and the 680-nm emission from Sm^{2+} with confocal detection implemented. We confirmed that the spacing of 2 μm between alphabetical character planes was sufficient to prevent cross-talk in the photoluminescence images. Although the 3D memory bits (photoreduced areas) was recorded with a femtosecond laser, they could be read with a CW laser at 0.5 mW.

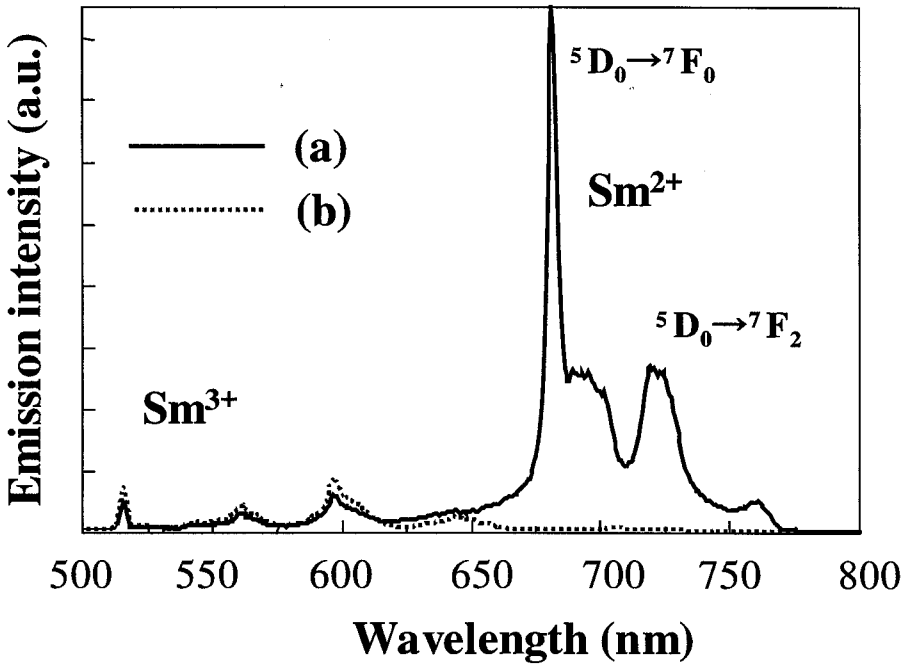

Fig.2.10. Photoluminescence spectra obtained by excitation at 488 nm for a laser-irradiated area (a) and non-irradiated area (b) in the interior of the glass.

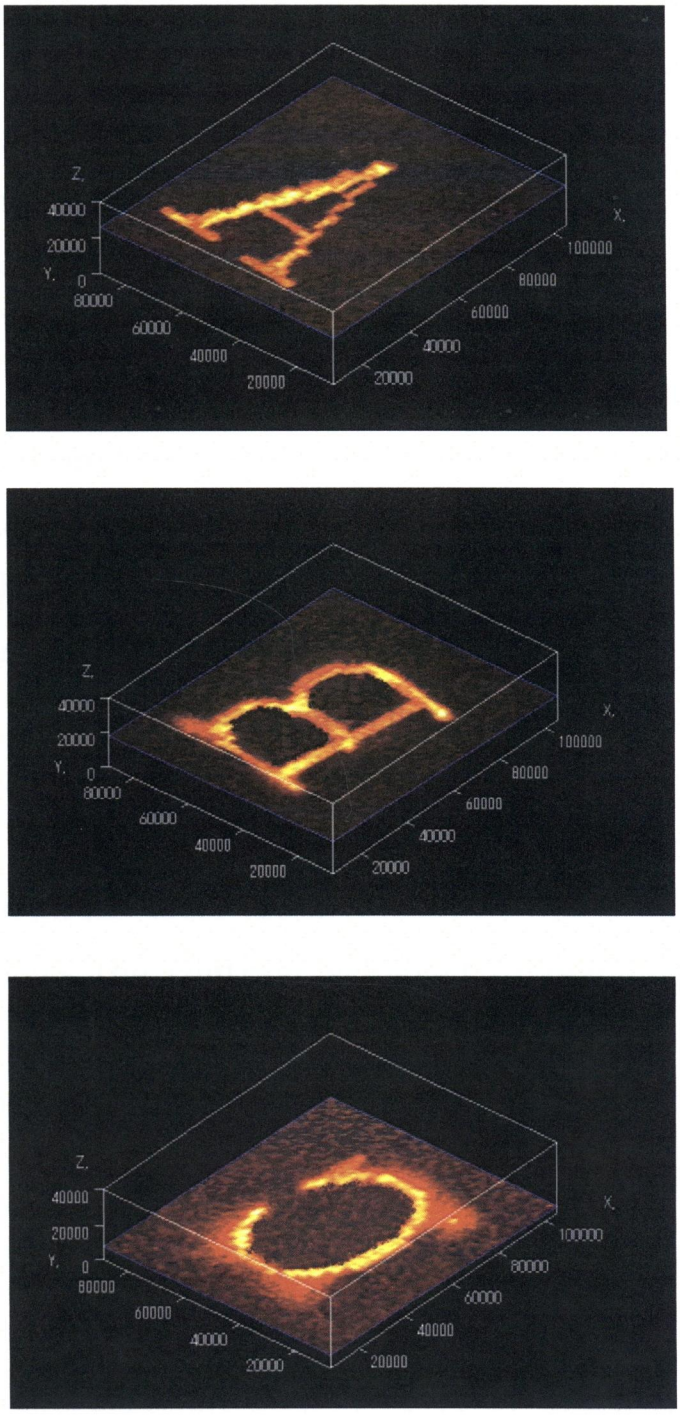

Fig. 2.11. Photoluminescence images of alphabetical characters recorded on different layers, which were observed by using a 40X objective lens and the 680-nm emission from Sm^{2+} with confocal detection implemented (excitation at 488 nm, 1-mW Ar^{+} laser).

Recording and readout in a three-dimensional memory are possible without any influence from bits in upper or lower layers recorded previously. Although obtaining a multilayer of several hundred layers has been difficult in a conventional 3D memory, it can be achieved by applying photoreduction bits to current optical memory technology. In addition, as shown in Fig.2.12, photoreduction bits with a 200-nm diameter could also be read out clearly by detecting the fluorescence as a signal. Since photoreduction bits can be spaced 150 nm apart on a layer in glass, a memory capacity of as high as 1 Tbit could be achieved for a glass piece with dimensions of 10mm x 10mm x 1 mm.

Another outstanding characteristic of the photoreduction of Sm^{3+} to Sm^{2+} is that stable Sm^{2+} at room temperature can be changed to Sm^{3+} by photooxidation with a CW laser, such as an argon ion laser or a semiconductor laser. An example of a photoreduction bit erased by irradiation with an Ar^{+} laser (10-mW at 514.5 nm) is shown in Fig.2.13. Figure 2.14 shows the contrast achieved in readout of bits (I, II) in Fig.2.13. These results indicate the possibility of achieving a three-dimensional optical memory with rewritable capability.

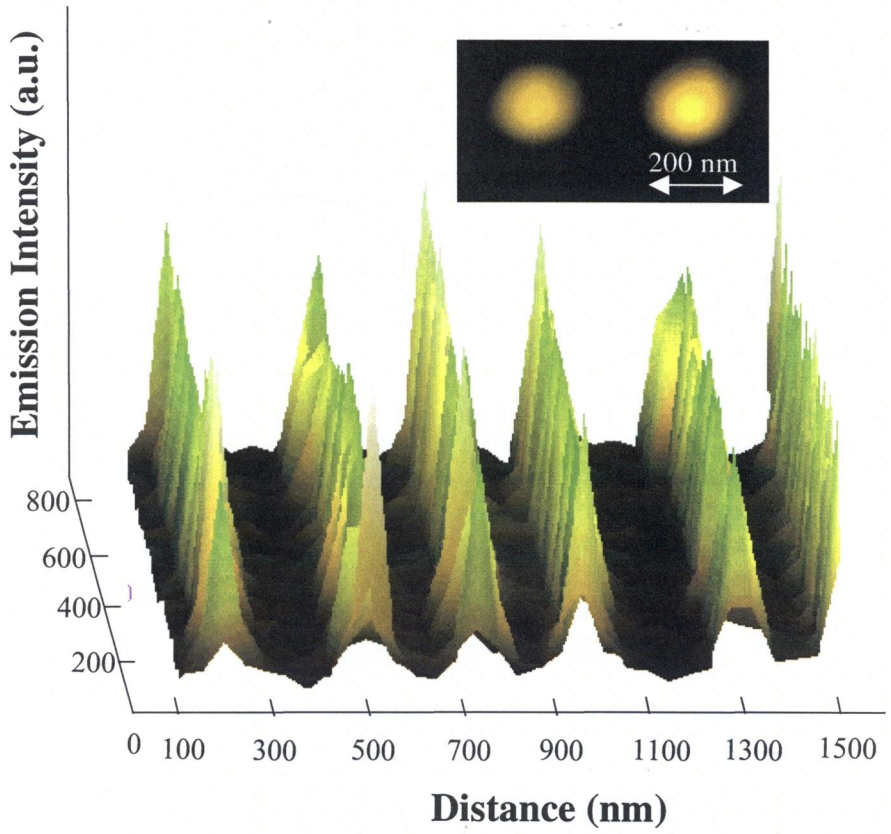

Fig. 2.12. Signal read out by detecting the fluorescence for photoreduction bits with a 200-nm diameter.

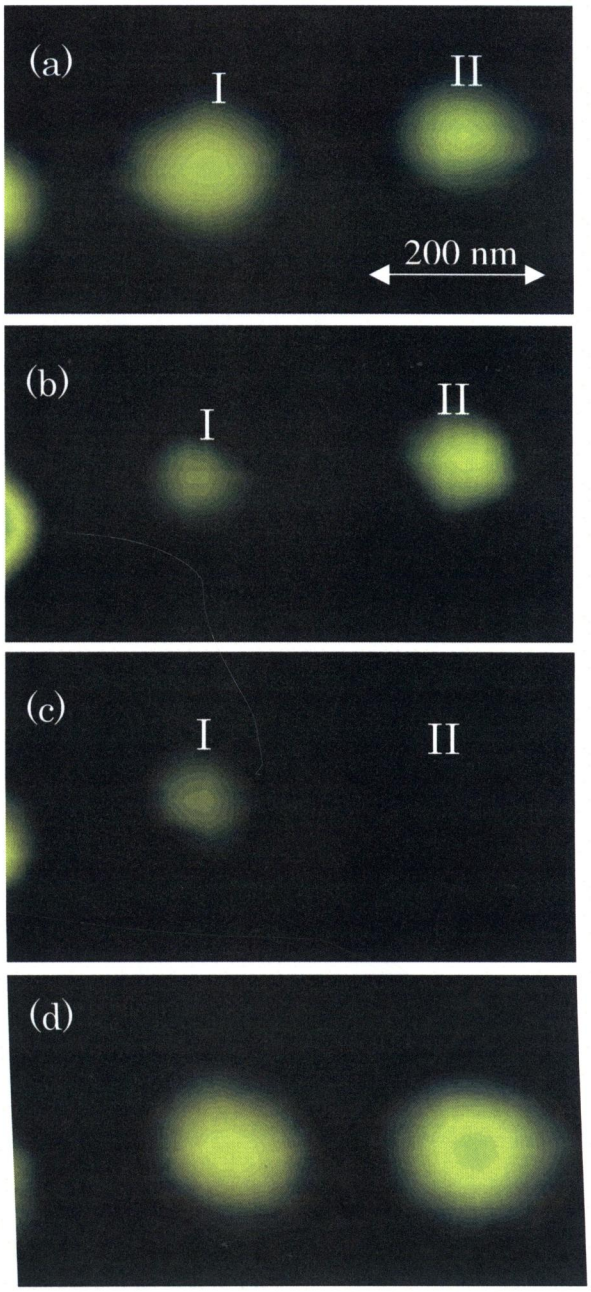

Fig. 2.13. An example of erasion and rewriting by irradiation with an Ar^+ laser (5-mW at 514.5 nm) and a femtosecond laser. (a) Photoluminescence image before the erasure. (b) Image after an Ar^+ laser irradiation to photoreduction bit I. (c) Moreover, image after an Ar^+ laser irradiation to bit II. (d) Image after a femtosecond laser irradiation to areas I and II.

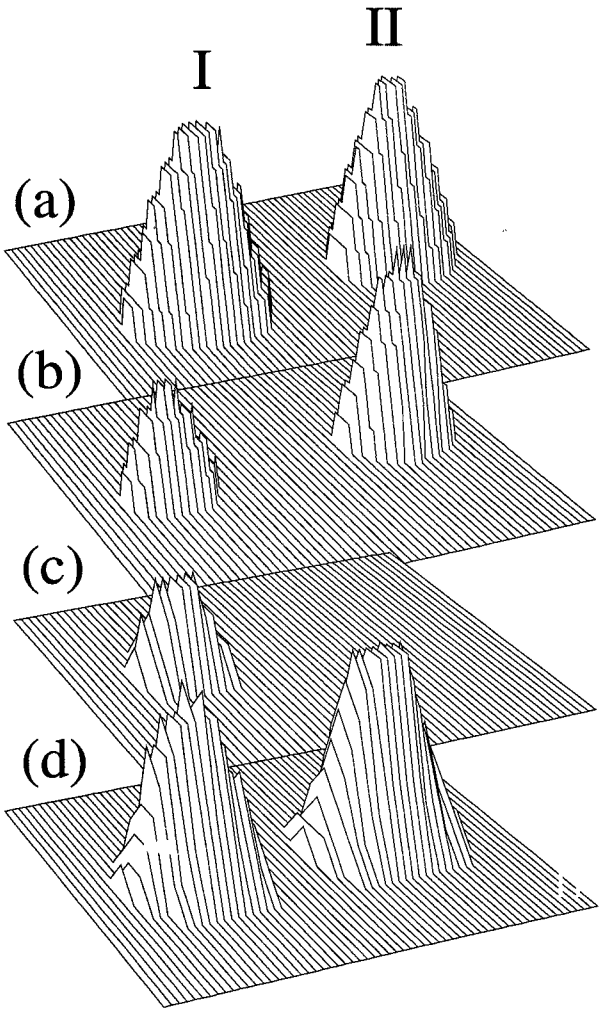

Fig. 2.14. Intensity distribution of the fluorescence (680 nm) for bits of I and II in Fig. 4 (a), (b), (c) and (d).

2.3.4 Conclusion

By using the valence state change of samarium ions to represent a bit, data can be read out as fluorescence information and erased by irradiation with a CW laser. The ratio of the fluorescence intensity at 680 nm after and before irradiation with the femtosecond laser is limitless, so a high signal-to-noise ratio can be achieved. Moreover, it is possible to create a multilayer record of data over several hundred layers, because the recording, readout and erasure processes for the data are not affected by layers recorded nearby. Therefore, this technique will be useful in fabricating next-generation 3D optical memory devices with an ultrahigh storage density.

References

[1] E. Snitzer, *Phys. Rev. Lett.* **7**, 444 (1961).

[2] Y. Ohishi, T. Kanamori, T. Kitayama, and S. Takahashi, *Opt. Lett.* **16**, 1747 (1991).

[3] M. Mitsunaga, R. Yano, and N. Uesugi, *Opt. Lett.* **16**, 1890 (1991).

[4] M. W. Shafer and J. C. Suits, *J. Am. Ceram. Soc.* **49**, 261 (1996).

[5] K. Hirao, S. Todoroki, D. H. Cho, and N. Soga, *Opt. Lett.* **18**, 1586 (1993).

[6] J. Qiu, Y. Shimizugawa, Y. Iwabuchi, and K. Hirao, *Appl. Phys. Lett.* **71**, 43 (1997)

[7] A. J. Cohen, H. L. Smith, *Science*, **336**, 89 (1962).

[8] H. Hosono, Y. Yamazaki, and Y. Abe, *J. Am. Ceram. Soc.* **70**, 867 (1987).

[9] T. Kanou, in *Handbook of Phosphors, Keikoutaido-gakukai,* ed. (Ohm, Tokyo, 1987), p. 110; in Japanese

[10] M. D. Feit, A. M. Rubenchik, B. W. Shore, and M. D. Perry, *Phys. Rev. Lett.* **74**, 2248 (1995).

[11] T. Kushida, in *Optical Physics* (Asakura Press, Tokyo, 1992), p.176. in Japanese

[12] M. W. Shafer, J. C. Suits, *J. Am. Ceram. Soc.* **49**, 261 (1996).

[13] J. Qiu, K. Tanaka, and K. Hirao, *J. Am. Ceram. Soc.* **80**, 2696 (1997).

[14] K. Hirao, S. Todoroki, D. H. Cho, and N. Soga, *Opt. Lett.* **18**, 1586 (1993).

[15] A. J. Cohen and H. L. Smith, *Science*, **336**, 89 (1962).

[16] T. Donohue, in *Chemical and Biochemical Applications of Laser*, edited by C. B. Moore (Academic, New York, 1980),p. 239

[17] M. Kusaba, T. Tswnawaki, W. Kawamura, Y. Izawa, and C. Yamanaka, *J. Photochem. Photobiol.*, A **104**, 55 (1997).

[18] M. Kusaba, W. Kawamura, T. Tswnawaki, Y. Izawa, and C. Yamanaka, *Chem. Phys. Lett.* **197**, 136 (1992)

[19] K. Hirao, *J. Non-Cryst. Solids* **196**,16 (1996).

[20] K. Nakagawa, in *Glass Dictionary*, edited by S. Sakka (Asakura, Tokyo, 1985), p.362. in Japanese

[21] B. C. Stuart, M. D. Feit, A. M. Rubenchik, B. W. Shore, and M. D. Perry, *Phys. Rev. Lett.* **74**, 2248 (1995).

[22] M. Watanabe, S. Juodkazis, H.-B. Sun, S. Matsuo, and H. Misawa, *Appl. Phys. Lett.*, **77** 13 (2000).

[23] K. Yamasaki, S. Juodkazis, M. Watanabe, H.-B. Sun, S. Matsuo, and H. Misawa, *Appl. Phys. Lett.*, **76** 1000 (2000).

[24] D. Homoelle, S. Wielandy, and Alexander L. Gaeta, *Opt. Lett.*, **24**, 1311 (1999).

[25] W. Denk, J. H. Strickler, and W. W. Webb, *Science* **248**, 73 (1990).

[26] Y. Kawata, H. Ishitobi, and S. Kawata, *Opt. Lett.* **23**, 756 (1998)

[27] E. N. Glezer, M. Milosavljevic, L. Hung, R. J. Finlay, T.-H. Her, J. P. Callan, and E. Mazur, *Opt. Lett.* **21**, 2023 (1996).

Chapter 3

Mechanisms and applications of space-selective growth of frequency-conversion crystals in various glasses by femtosecond laser irradiation

3.1 Introduction

So far ultrashort laser pulses are useful for observing and evaluating at a very high time resolution the dynamics of phenomena that occur within materials at speeds ranging from picoseconds to femtoseconds [1-3]. Such phenomena include direct interaction between light and atoms or molecules, the saturation process associated with the coherent state of materials, and the elementary process of chemical reactions. On the other hand a short pulse width gives an extremely high intensity power up to 10^{14} W/cm^2 at a focal point of the laser. Therefore, the development of high-energy-density femtosecond pulse lasers would prompt us to investigate the unexplored potential for inducing multiphoton photochemical reactions. That means there is considerable interest in using femtosecond lasers to generate various kinds of interactions with many types of materials, especially in metastable glass.

In Chapter 1 and 2, it was observed that a variety of photo-induced structure changes that are permanent at room temperature can be produced only near the beam focusing area inside bulk glasses with femtosecond laser pulses. When we irradiate the interior of the material with an ultrashort pulse (femtosecond order), energy is accumulated at a minute area for a very short time. This might be caused by such effects as ionization and plasma vibration, which are presumed to produce a dramatic rise in the temperature and internal pressure in the region of focus [4]. In taking advantage of this

phenomenon, we could form spherical melting regions at arbitrary sites within a bulk glass, and for the first time succeed in growing single crystals with special components from the melt. This letter describes how we succeeded to grow BBO (β-BaB_2O_4) with excellent characteristics inside a bulk glass by a novel method using a nonresonant ultrashort pulse laser. This BBO (β-BaB_2O_4) exhibits excellent performance when applied to frequency conversion devices, especially in the UV region.

3.2 Experimental procedure

The glass used in this study was prepared with components of BaO, TiO_2 and B_2O_3. We tightly focus femtosecond laser pulses inside a bulk glass to create localized nonlinear optical crystals of BBO. The irradiation sources employed were a regeneratively amplified 800-nm Ti:sapphire laser that emitted 4μJ, 130 fs, 200-kHz mode-locked pulses. A microscope system was used to tightly focus the laser pulses inside the glass sample to grow localized frequency conversion crystals.

3.3 Results and Discussion

When the laser beam was focused in the interior of the samples, however, no cracking was detected and the only atomic scale damage observed was that resulting from various phenomena such as the formation of color centers or lattice defects (a), local densification (b) or melting of a very small (c) area (see Fig. 3.1). (If we use a nanosecond laser instead of a femtosecond laser, cracking due to thermal shock occurs at a focal point of a nanosecond-order laser pulse in the interior of the glass samples.) After the short period irradiation, frequency conversion crystals can be generated near the focal point of a laser beam under irradiation conditions such as those shown in Fig. 3.1(c). By using the photosensitivity attributed to the nonlinear optical process, visible laser damage was formed only inside the focused region, because

nonlinearity occurs only in regions with high optical intensity above the damage threshold. Figure 3.2 shows microscopic photographs taken near the focal point directly after focused irradiation of (a) 0 minutes, (b) 20 minutes and (c) 30 minutes after irradiation of the laser (wavelength: 800 nm, repetition frequency: 200 kHz, average output: 600 mW) in $BaO\text{-}TiO_2\text{-}B_2O_3$ glass via an 50 × objective lens. From the measurement of X-ray diffraction patterns, it was confirmed that only BBO crystals were grown in the laser focused area [see Fig. 3.3]. In a similar way, we confirmed that it is possible to generate other frequency conversion crystals of $LiNbO_3$ crystal from $Li_2O\text{-}K_2O\text{-}Nb_2O_5\text{-}SiO_2$ glass using a femtosecond laser.

Figure 3.4 shows the variation of emission spectra obtained from moving the laser focal point that accompanies growth of frequency conversion crystals. Although only broadening of 800 nm femtosecond laser pulses due to self-phase modulation was observed immediately after laser irradiation, with the passage of time, it was confirmed that the intensity of second harmonic generation increases with the growth of frequency conversion crystals. In addition, after frequency conversion crystals are created by femtosecond laser irradiation, second harmonic generation of blue laser can also be observed by the incidence of an infrared nanosecond-order pulse laser. A spectrum of second harmonic generation from frequency conversion crystals observed by the incidence of 800 nm nanosecond laser pulses is shown in Fig. 3.5.

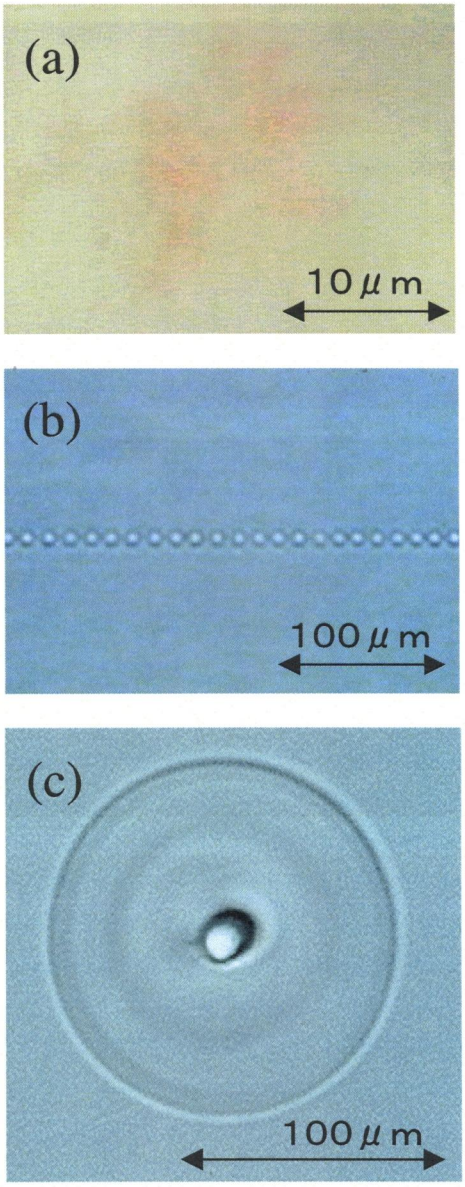

Fig. 3.1. Damages caused by focusing a femtosecond laser in the interior of the glass. (a) Damage in the interior caused by 1-μJ pulses focused through a lens of 100-mm focal length. (b) Damage in the interior caused by 1-μJ pulses focused through a 10X objective lens. (c) Damage in the interior caused by 4 -μJ pulses focused through a 50X objective lens. Each sample received 200,000 pulses/spot through a microscope objective.

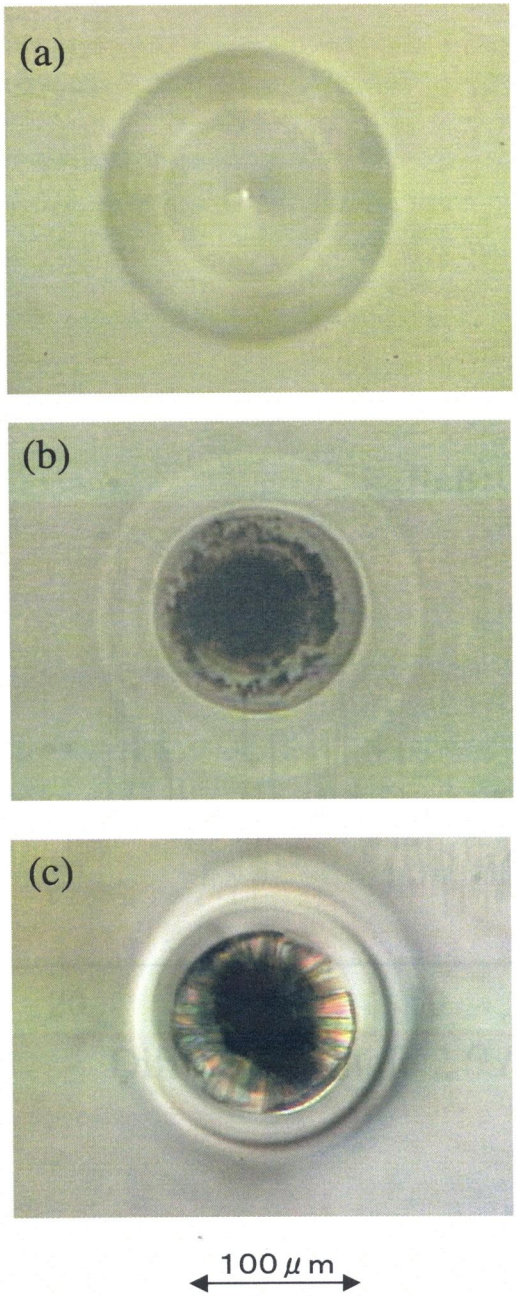

Fig. 3.2. Microscopic photographs taken near the focal point directly after focused irradiation (a), 20 minutes (b) and 30 minutes (c) after irradiation. Wavelength, average power and pulse width of the laser were 800 nm, 600 mW and 130 fs at 200 kHz, respectively.

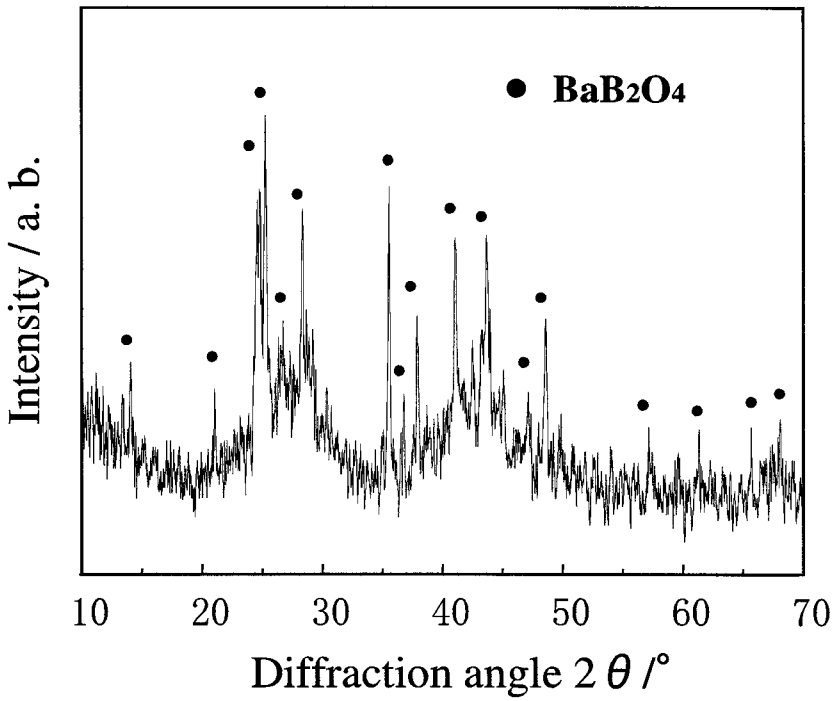

Fig. 3.3. X-ray diffraction pattern for crystals created by the irradiation of focused laser beam with 50X microscope objective, an average power 800 mW, and a irradiation time of 40 minutes.

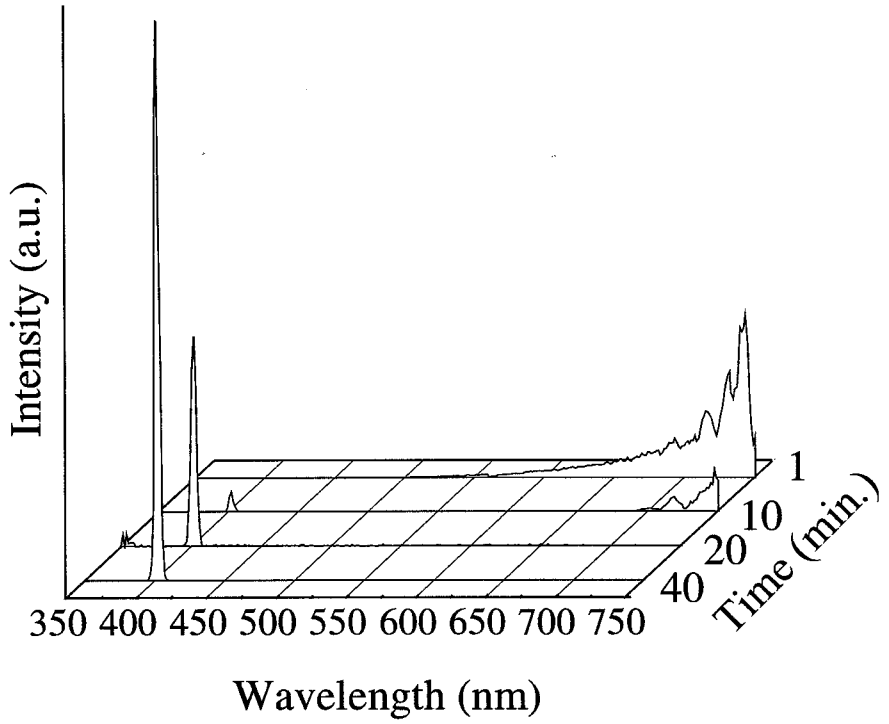

Fig. 3.4. Variation of emission spectra obtained from the laser focal point that accompanies growth of frequency conversion crystals for various irradiation times. Wavelength, average power and pulse width of the irradiation laser were 800 nm, 450 mW and 130 fs at 200 kHz, respectively.

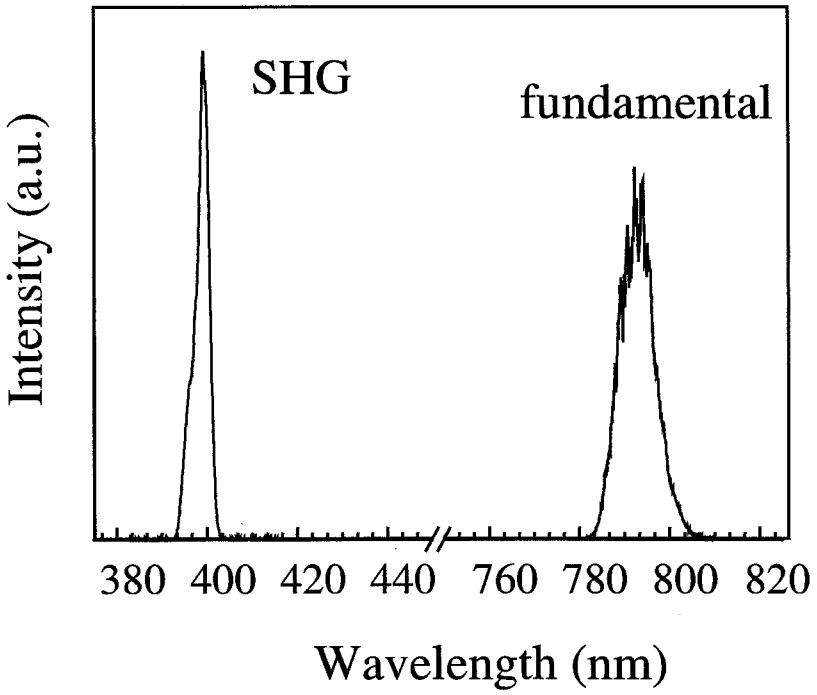

Fig. 3.5. Spectrum of second harmonic generation from frequency conversion crystals observed by the incidence of 800 nm nanosecond laser pulses.

Moving the focal point of a laser beam relative to the position of the glass sample enables the melting region to move freely. We attempted to generate frequency conversion crystals continuously inside the glass by moving the melting zone. Polarizing microscope photographs of the side (a), (b) and cross-sectional (c) views of the crystal were shown in Fig. 3.6. In this figure, (a) and (b) show polarizing-microscope photographs taken in extinction and diagonal positions, respectively. Region A in cross-section photo (a) shows a crystal grown while moving the melting zone at a speed of 100 μm/s, while region B shows a crystal grown when this speed is 10 μm/s. The melting zone was moved continuously from region A to region B. The glass layer situated at the periphery of the grown crystal constitutes an area whose structure has changed due to the crystallization of specific components in the glass. The crystal of region A is clearly a polycrystal due to the existence of grain boundaries revealed by a change in interference color. Surprisingly on the other hand, the crystal of region B exhibits hardly any grain boundaries indicating a crystal having a fixed orientation. The above phenomenon indicates that by decreasing the movement speed of the fusion zone, a stable structure having an accommodation layer is formed at the solid-liquid interface between a part of the polycrystal in region A and the fusion zone. It means that this technique gives the growth of a single crystal or a crystal with a single-crystal-like structure. By using seed-crystals in the phase matching direction, it is possible to grow crystals adequate for use in frequency conversion devices.

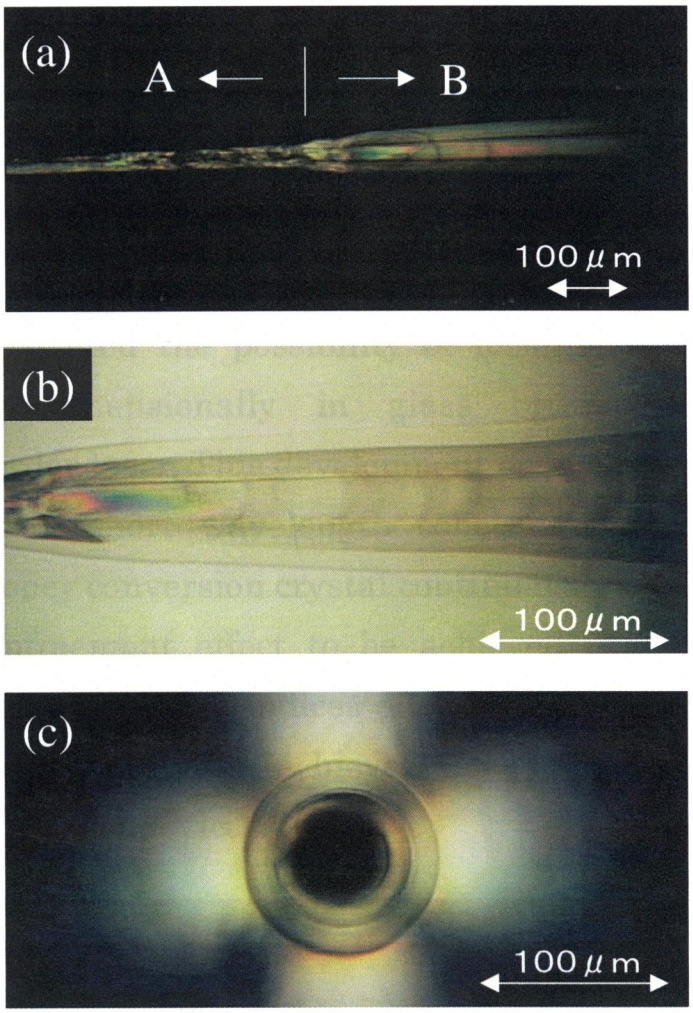

Fig. 3.6. Polarizing microscope photographs of the side (a), (b) and cross-sectional (c) views of the crystal. (a) and (b) show polarizing-microscope photographs taken in extinction and diagonal positions, respectively. Region A in cross-section photo (a) shows a crystal grown while moving the melting zone at a speed of 100 μm/s and region B shows a crystal grown when this speed is 10 μm/s.

3.4 Conclusion

In an attempt to grow three-dimensional frequency conversion crystals in any direction in bulk glasses, we have investigated various photo-induced phenomenon created by focusing an femtosecond laser having a ultra-short laser pulse through a microscope objective, and demonstrated that frequency conversion of single-crystals could successfully be grown in the glass through our new novel method. Our results demonstrated the possibility of forming frequency conversion crystals three-dimensionally in glass by using a nonresonant femtosecond-order laser. This development opens new possibilities in the field of compact short wavelength coherent light sources. Further, forming frequency conversion crystal continuously in glass should enable an optical confinement effect to be achieved that makes use of the difference in the refractive indices of the glass and the crystals, which may make it possible to achieve new waveguide nonlinear-optic frequency conversion devices.

References

[1] F.M. Peter and H.A. Zewail, *Phys. Rev. Lett.* **53**, 501 (1984).

[2] M.P. Felker and A. Zewail, *Phys. Chem.* **91**, 754 (1987).

[3] C. Rischel , *Nature* **390**, 490 (1997).

[4] Y. Shuto, H. Tanaka, M. Amano, T. Kaino, *Jpn. J. Appl.Pkys.*, **28**, 2508 (1989).

Summary

In the present study, the various microscopic modifications in glasses by ultra-short pulses were investigated. It was confirmed that permanent refractive index changes, the phenomenon of long-lasting phosphorescence, photo-reduction of samarium ions, and the creation of frequency conversion crystal can be produced with a femtosecond pulse laser only in selective internal areas in glasses. By using a femtosecond laser with a high repetition rate, permanent optical waveguides can be successfully written in various glasses, where refractive index changes are continuously induced along a path traversed by the focal point. The possibility of achieving 3D optical data storage inside glass by using a focused femtosecond laser to permanently photoreduce of Sm^{3+} to Sm^{2+} was also examined. The results of the respective Chapter are summarized as follows.

In Chapter 1, with the goal of being able to create optical devices for the telecommunications industry, the effects of the femtosecond laser irradiation inside various glasses. Microellipsometer measurements of the laser irradiation region in pure and Ge-doped silica glasses showed a 0.01-0.035 refractive index increase, depending on the radiation dose. The formation of several defects, including Si E' and Ge E' centers, non-bridging oxygen hole centers, and peroxy radicals, was also detected. These results suggest that multiphoton interactions occur in the glasses.

The confocal microscopic Raman scattering and AFM on the photo-induced refractive index change in SiO_2 glass with an ultra-short pulse laser were measured. We proved that the increase in refractive index caused by the ultra-short pulse laser could be related to the local densification in the glasses. It is also clear that laser irradiation reconstructs the glass structure.

In an attempt to write optical waveguides in bulk glasses,

photo-induced refractive index changes were continuously created by focusing an ultra-short pulse laser through a microscope objective and translating the sample parallel to the axis of the laser beam. The resulting, linear refractive index changes were written inside the bulk glasses along the path traversed by the focal point of the laser. From field intensity distributions in the output of guided light for these waveguides, we demonstrated that permanent optical waveguides could be successfully formed in various types of glass. In addition, through analyzing the near-field pattern with a CCD camera, we confirmed that single mode waveguides of the graded index type could be formed by a writing technique using an ultra-short pulse laser. These facts open new possibilities in the field of integrated optics and three-dimensional optical circuits, especially for the conception of compact, all-solid-state lasers, amplifiers, and optical switches.

In Chapter 2, two novel phenomena in the glasses doped with rare-earth ions were reported as follows.

Femtosecond infrared laser-induced long-lasting phosphorescence in Ce^{3+}-, Tb^{3+}-, and Pr^{3+} -doped calcium aluminosilicate glasses was observed. The long-lasting phosphorescence is considered to be due to the thermal stimulated recombination of holes and electrons at traps induced by the laser irradiation, which leave holes or electrons in a metastable excited state at room temperature. We suggest that it may be possible to selectively induce defects by using lasers with different wavelengths, pulse widths, and repetition rates. The energy due to the recombination of holes and electrons in various defects may be different and selectively excite the electrons in the ground state to an excited state of rare earth ions, e.g., Pr^{3+}, leading to the occurrence of phosphorescence in various colors in a glass.

The permanent photo-reduction in Sm^{3+} to Sm^{2+} in a sodium aluminoborate glass by 800 nm femtosecond laser pulses was observed. Absorption and photoluminescence spectra showed that a part of Sm^{3+}

was reduced to Sm^{2+} after the laser irradiation.

The recording, readout and erasure of a three-dimensional optical memory using the valence-state change of samarium ions to represent a bit was also reported. A photoreduction bit of 200 nm diameters can be recorded with a femtosecond laser and readout clearly by detecting the fluorescence as a signal (excitation at 488 nm, 0.5-mW Ar^+ laser). A photoreduction bit that is stable at room temperature can be erased by photooxidation with a CW laser (514.5 nm, 10m-W Ar^+ laser). Since photoreduction bits can be spaced 150 nm apart in a layer within glass, a multilayer structure with several hundred layers could be used to record data. A memory capacity of as high as 1 Tbit could thus be achieved in a glass piece with dimensions of 10 mm x 10 mm x1 mm. The ratio of the fluorescence intensity at 680 nm after and before irradiation with the femtosecond laser is limitless, so a high signal-to-noise ratio can be achieved. This technique will be useful in fabricating next-generation 3D optical memory devices with an ultrahigh storage density.

In Chapter 3, at the focal point of an 800-nm femtosecond laser beam, the space-selective growth of second-harmonic-generation β-BaB_2O_4 (BBO) crystal inside a BaO-Al_2O_3-B_2O_3 glass sample was reported. A spherical heated region was formed during the focused laser irradiation through observation with an optical microscope. We moved the heated region by changing the position of the focal point of the laser beam relative to the glass sample. We grew BBO crystal continuously in the glass sample by adjusting the moving speed of the heated zone. Our results demonstrate the possibility of forming frequency-conversion crystals three dimensionally in glass by use of a nonresonant femtosecond-order laser. This development opens new possibilities in the field of compact short-wavelength coherent light sources. Further, the forming of a continuous frequencyconversion crystal in glass should permit an optical confinement effect to be achieved that makes use of the difference in the refractive indices of the glass and the crystals, which

may make it possible to achieve new waveguide-type nonlinear-optic frequency-conversion devices.

List of publications

Chapter 1

K.M.Davis, K.Miura, N.Sugimoto, and K.Hirao
"Writing Waveguides in Glass with a Femtosecond Laser"
Opt. Lett., **21**, 1729-1731 (1996).

K.Miura, J.Qiu, H.Inouye, T.Mitsuyu, and K.Hirao
"Photowritten Optical Waveguides in Various Glasses with Ultrashort Pulse Laser"
Applied Physics Letters, **71**, 3329-3331 (1997).

K.Miura, J.Qiu, T.Mitsuyu, and K.Hirao
"Preparation and Optical Properties of Fluoride Glass Waveguides induced by Laser Pulses"
Journal of Non-Crystalline Solids, **256,,** 212-219 (1999).

Chapter 2

K.Miura, J.Qiu, T.Mitsuyu, and K.Hirao
"Three-dimensional Microscopic Modifications in Glasses by a Femtosecond Laser"
Proceedings of SPIE Reprint, **3618**, 141-151 (1999).

J.Qiu, K.Miura, H.Inouye, Y.Kondo, T.Mitsuyu, and K.Hirao
"Femtosecond Laser-induced Three-dimensional Bright and Long-lasting Phosphorescence inside Calcium Aluminosilicate Glasses Doped with Rare Earth Ions"
Applied Physics Letters, **73**, 1763-1765 (1998).

J.Qiu, K.Miura, T.Suzuki, T.Mitsuyu, and K.Hirao
"Permanent Photoreduction of Sm^{3+} to Sm^{2+} inside a Sodium

Alminoborate Glass by an Infrared Femtosecond Pulsed Laser"
Applied Physics Letters, **74**, 10-12 (1999).

K.Miura, J.Qiu, S.Fujiwara, S.Sakaguchi, and K.Hirao,
"Three-dimensional optical memory with rewriteable and ultrahigh density using valence state change of samarium ions"
Applied Physics Letters, **180**, 2263-2265 (2002).

Chapter 3

K. Miura, J. Qiu, T. Mitsuyu, and K. Hirao
"Space-selective growth of frequency-conversion crystals in glasses with ultrashort infrared laser pulses"
Optics Letters, **125**, 408-410 (2000).

Other publications not contained in this thesis

1. J. Qiu, K. Miura, N. Sugimoto, and K. Hirao
   Preparation and Fluorescence Properties of Fluoroaluminate Glasses Containing Eu^{2+} ions
   Journal of Non-Crystalline Solids, **213 & 214**, 266-270 (1997).
2. K.Miura and K.Hirao
   Photo-induced Refractive Index Changes in Glasses with Ultra-short Pulse Laser
   The Review of Laser Engineering, **26** (2), 150-154 (1998).
3. K.Hirao and K.Miura
   Writing Waveguides in Silica-related Glasses with Femtosecond Laser
   Japanese Journal of Applied Physics, **37**, 49-52 (1998).
4. J.Qiu, K.Miura, and K.Hirao
   Three-dimensional Optical Memory Using Glasses as a Recording Medium through a Multi-photon Absorption Process
   Japanese Journal of Applied Physics, **37**, 2263-2266 (1998).
5. J.Qiu, K.Miura, H.Inouye, J.Nishii, K.Hirao
   Three-demensional Optical Storage inside a Silica Glass by Using a Focused Femtosecond Pulsed Laser
   Nuclear Instruments and Methods in Physics Research B, **141**, 699-703 (1998).
6. K.Miura, H.Inouye, J.Qiu, T.Mitsuyu, and K.Hirao
   Optical Waveguides Induced in Inorganic Glasses by a Femtosecond Laser
   Nuclear Instruments and Methods in Physics Research B, **141**, 726-732 (1998).
7. K.Hirao and K.Miura
   Writing Waveguides and Gratings in Silica and Related Materials by a Femtosecond Laser
   Journal of Non-Crystalline Solids, **239**, 91-95 (1998).

8. Y.Kondo, T.Suzuki, H.Inouye, K.Miura, T. Mitsuyu, and K.Hirao
Three-dimensional Microscopic Crystallization in Photosensitive Glass by Femtosecond Laser Pulses at Nonresonant Wavelength
Japanese Journal of Applied Physics, **37**, 94-96 (1998).

9. Peter G. Kazansky, H.Inouye, T.Mitsuyu, K.Miura, J.Qiu, and K.Hirao
Anomalous Anisotropic Light Scattering in Ge-doped Silica Glass
Physical Review Letters, **82**, 2199-2202 (1999).

10. J.Qiu, K.Kojima, K.Miura, T.Mitsuyu, and K.Hirao
Infrared Femtosecond Laser Pulse-induced Permanent Reduction of Eu^{3+} to Eu^{2+} in a Fluorozirconate Glass
Optics Letters, **24**, 786-788 (1999).

11. J.Qiu, Y.Kondo, K.Miura, T.Mitsuyu, and K.Hirao
Infrared Femtosecond Laser Induced Visible Long-lasting Phosphorescence in Mn^{2+}-doped Sodium Borate Glasses
Japanese Journal of Applied Physics, **38**, L649-L651 (1999).

12. Y.Kondo, K.Miura, T.Suzuki, H.Inouye, T.Mitsuyu, K.Hirao
Three-dimensional Arrays of Crystallites within Glass by Using Non-resonant Femtosecond Pulses
Journal of Non-Crystalline Solids, **253**, 143-156 (1999).

13. J.Qiu, N.Kodama, M.Yamada, K.Miura, T.Mitsuyu, and K.Hirao
Infrared Femtosecond Laser Pulse-induced Three-dimensional Bright and Long-lasting Phosphorescence in a Ce^{3+}-doped $Ca_2Al_2SiO_7$ Crystal
Journal of Applied Optics, **38**, 7202-7205 (1999).

14. J.Qiu, K.Miura, K.Nouchi, T.Suzuki, Y.Kondo, T.Mitsuyu, and K.Hirao
Valence Manipulation by Lasers of Samarium ion in Micrometer-scale Dimensions inside Transparent Glass
Solid State Communications, **113**, 341-344 (2000).

15. J.Qiu, K.Miura, K.Nouchi, T.Suzuki, Y.Kondo, T.Mitsuyu, and K.Hirao
Valence Manipulation by Lasers of Samarium ion in Micrometer-scale Dimensions inside Transparent Glass
Solid State Communications, **113**, 341-344 (2000).

16. J. Qiu, K. Nouchi, K. Miura, T. Mitsuyu, and K. Hirao,
Room-temperature Persistent Spectral hole Burning of X-ray-irradiated Sm^{3+}-doped Glass
Journal of Physics: Condens. Matter., **12**, 5061-5067 (2000).
17. J. Qiu, P. G. Kazanski, J. Si, K. Miura, T. Mitsuyu, K. Hirao, A. and L. Gaeta
Memorized Polarization-dependent Light Scattering in Rare-earth-ion-doped Glass
Applied Physics Letters, **77**, 1940-1942 (2000) .

Acknowledgement

The present thesis has been carried out under the direction of Professor Kazuyuki Hirao at Graduate School of Engineering in Kyoto University.

First of all, the author wishes to express special thanks to Professor Kazuyuki Hirao, who supervised the present work, for his helpful direction and encouragements. The author also thanks Professor Toshinobu Yoko and Professor Masahiro Kawasaki for their instructive suggestions.

Grateful acknowledgements are made to Dr. Jianrong Qiu, Photon Craft Project (ICORP, JST), for his valuable suggestions and helpful discussions. The profitable suggestions from Professor Kazuki Nakanishi and Dr. Koji Fujita are also gratefully acknowledged. The author also thanks Professor Masahide Terazima and Mr. Masaaki Sakakura of his laboratory for helpful advice in measurement of photoluminescence. The author is indebted to Dr. Jinhai Si at Photon Craft Project (ICORP, JST) and his co-workers for their collaboration. The author also wishes to thank Dr. Hideyuki Inouye at Nara Institute of Science and Technology for his helpful advice, and Dr. I. Kudryashov of Tokyo Instruments, Inc. for his kind help in the using of photoluminescence. Hearty thanks are made to all the students and staffs of Hirao's laboratory for their helpful discussion and excellent assistance.

Finally, The author acknowledges his co-workers, Mr. Seizi Fujiwara of NEC Corporation, Mr. Natsuya Nishimura of Central Glass Co., Ltd., for their support and encouragement.

Kyoto, Winter 2003 Kiyotaka Miura